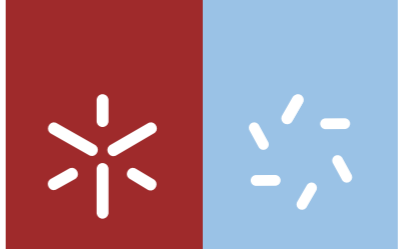


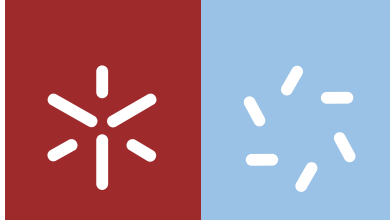


Microfluidic methods for the controlled
preparation of soft self-assembled
nanocarriers for drug delivery

Celso Joel Oliveira Ferreira

Universidade do Minho
Escola de Ciências





Universidade do Minho
Escola de Ciências

Celso Joel Oliveira Ferreira

**Microfluidic methods for the controlled
preparation of soft self-assembled
nanocarriers for drug delivery**

Master thesis
Master in Biophysics and Bionanosystems

Work developed under supervision of
Dr. Bruno Fernando Brás da Silva
INL-International Iberian Nanotechnology Laboratory

Prof. Maria Elisabete da Cunha Dias Real Oliveira
Universidade do Minho

DECLARATION

Name: Celso Joel Oliveira Ferreira

Email: celso_joelferreira@hotmail.com

Phone: 915659658

ID nº: 14861153

Thesis title: Microfluidic methods for the controlled preparation of soft self-assembled nanocarriers for drug delivery

Supervisors:

Dr. Bruno Fernando Brás Da Silva

Prof. Maria Elisabete da Cunha Dias Real Oliveira

Conclusion year: 2018

Master course: Master in Biophysics and Bionanosystems

IN ACCORDANCE WITH CURRENT LEGISLATION, THE
REPRODUCTION OF ANY PART OF THIS THESIS / WORK
IS NOT PERMITTED

University of Minho, October 2018

Signature: Celso Joel Oliveira Ferreira

Acknowledgements

To my supervisor at INL, Dr. Bruno Fernando Brás da Silva for accepting me in this journey, for the knowledge shared, motivation, patience, optimism, persistence, and of course for providing me with the best work opportunity one could have.

To my supervisor at University of Minho, Professor Maria Elisabete Cunha Dias Real Oliveira for allowing me to enrol in this work, for teaching me and for being always so kind and optimistic.

For Cláudia Botelho, Joana Margarida and Vahid Nasirimarekani, for all the help, knowledge, encouragement and funny conversations.

To all the microfluidics group, Paulina Piairo, Lei Wu, Krishna Kant, Sara Abalde and Sandra Carvalho, for helping whenever I needed, for being always in the best mood possible and of course for the best after work events.

To my university colleagues who accompanied me along this journey, Marisol, Magda, Irina and Mário, thank you for the good moments spent.

To my closest friends, João Nuno, João Queirós, Filipe, Guarani, Luís Silva, Eduardo, Tiago Foz and Tiago André, whether for the personal conversations, or for the craziest adventures, thank you.

To my beloved family, my mother Paula Manuela Afonseca Oliveira, my father Abílio dos Santos Ferreira and my brother Tomás Oliveira Ferreira, for the life lessons, for believing in me and pushing me forward no matter the situation.

For Cláudia Marisa da Silva Machado and Pedro Manuel Lima da Silva, for not only being by my side, but for the funny moments, the companionship and of course, for the help provided when I most needed.

To all my friends and colleagues, thank you!

Resumo

Cubossomas são dispersões lipídicas de fases cúbicas bicontínuas em água. Estas partículas possuem no seu interior uma matriz de bicamadas lipídicas arranjadas numa rede tridimensional contínua de simetria cúbica que separa duas redes contínuas de canais de água. Tal coexistência de domínios lipídicos e aquosos faz dos cubossomas excelentes candidatos para a encapsulação e entrega de compostos hidrofóbicos e hidrofílicos.

Os cubossomas são geralmente preparados quer por fragmentação da fase bicontínua cúbica em excesso de água ao introduzir uma grande quantidade de energia (como por exemplo ultra-sonicação), ou então por uma troca de solventes, no qual o lípido é primeiramente dissolvido num solvente miscível em água (tipicamente o etanol), e mais tarde dissolvido em água e um polímero estabilizante. Em ambos os casos, um fraco controlo experimental à micro e nano-escala (e.g. fraco controlo nos gradientes de concentração e temperatura), limita a manipulação das propriedades das partículas e resulta em cubossomas com amplas distribuições de tamanho. Neste trabalho, o método da troca de solventes é aplicado ao sistema monooleína-etanol-água para formar cubossomas. Para este fim, um dispositivo de microfluídica capaz de misturar os solventes rápida e controladamente à microescala, e obter cubossomas com tamanhos manipuláveis e baixa polidispersão, foi usado.

Os canais à microescala usados nos dispositivos de microfluídica fazem com que o regime de fluxo seja laminar e reforce o controlo experimental. Neste regime, a focagem hidrodinâmica pode ser usada para diminuir a distância que as moléculas têm de atravessar para se misturarem, o que leva a uma diminuição no tempo de mistura. Uma solução de lípido-etanol é inserida pela entrada central, onde será de seguida espremida por dois fluidos laterais de água com estabilizante. À medida que a solução de lípido-etanol é espremida, o etanol e a água vão sendo misturados de uma forma controlada por difusão, o que leva à formação dos cubossomas. Ao manipular o rácio dos diferentes caudais entre as diferentes soluções, a largura à qual a focagem hidrodinâmica se dá é ajustada, influenciando o tempo de associação entre as moléculas lipídicas de forma homogénea. Desta forma, ao manipular o rácio dos caudais, foi possível manipular o tamanho dos cubossomas, atingindo menores tamanhos quando a extensão da focagem hidrodinâmica foi aumentada (aumentando o rácio dos caudais). Conjuntamente, também foi observado que a composição das soluções iniciais também influencia o tamanho final das partículas. A concentrações superiores a 1 %(m/m) de lípido na solução de etanol, o controlo sobre

o tamanho das partículas é reduzido. Assim como a inclusão do surfactante catiónico brometo de dioctadecil dimetil amónio (DODAB), que na formulação também gerou partículas de grandes tamanhos de forma descontrolada. Por outro lado, a inclusão de 29 %(m/m) de água na solução de lípido-etanol levou a que se formassem partículas com tamanhos reduzidos, também de uma forma controlada e dependente do rácio entre os caudais dos fluidos. A contrastar, quando utilizado um rácio de estabilizante para lípido de 1:1 ou 3:1, os tamanhos finais obtidos não demonstraram diferenças significativas entre ambos os rácios. Resumindo, estes resultados sugerem que o tamanho dos cubossomas está diretamente dependente do ritmo ao qual as moléculas de solvente vão sendo trocadas até atingirem uma concentração crítica de água que induz a formação das partículas. Ao permitir um controlo preciso sobre a mistura e troca entre ambos os solventes, as técnicas de microfluídica assumem-se como uma forma promissora de manipular a estrutura e aumentar a eficiência dos sistemas de entrega de fármacos. O tamanho das nanopartículas é um fator chave na entrega de fármacos e a possibilidade de controlar o tamanho dos cubossomas é, portanto, um passo na direção do desenvolvimento de novas e mais eficientes formulações.

Abstract

Cubosomes are dispersions of lipid bicontinuous cubic phases in water. These particles consist of an interior continuous matrix of lipid bilayers arranged in a 3D lattice of cubic symmetry that separates two independent continuous networks of water channels. This coexistence of lipidic and aqueous domains makes cubosomes promising candidates for the encapsulation and delivery of both hydrophobic and hydrophilic drugs.

Cubosomes are typically prepared either by fragmenting the cubic liquid crystal in excess water using high energy input (e.g. ultra-sonication), or using solvent-shifting approaches, in which the lipid is first dissolved in a water-miscible solvent (typically ethanol), and later mixed with water and polymer stabilizer. In both cases, poor experimental control at the micron- and nanoscales (e.g. poor control on concentration and heat gradients), limits the fine tuning of the particle properties and results in cubosomes with broad size distributions. In this work, we employ the solvent-shifting method to the monoolein-ethanol-water system and form cubosomes. For this, a microfluidic device capable of mixing the fluids in a rapid and controlled way at the micron-scale, and obtaining cubosomes of tuneable size and low polydispersity, is used.

The micron-sized channels in microfluidics lead to laminar flow regimes and enhanced experimental control. In this regime, hydrodynamic focusing can be used to narrow down the length that solvent molecules have to travel to mix, thus decreasing the mixing time. An ethanol-lipid solution is flowed in a central inlet, which is squeezed by two side streams of water with stabilizer. As the lipid-ethanol solution narrows, ethanol and water are mixed in a controlled way by diffusion, leading to formation of cubosomes. By manipulating the flow rate ratio between the two solutions we manipulate the width in which the hydrodynamic focusing occurs, influencing the assembly time in a homogeneous way. This way, by manipulating the flow rate ratio, we were able to tune the size of the cubosome nanoparticles, achieving smaller sizes when increasing the extent of the hydrodynamic focusing (i.e. increasing the flow rate ratio). In addition, the final particle size was also found to be influenced by the composition of the initial solutions. At lipid concentrations above 1 wt% in the ethanolic solution, control over the final particle size is lost. Likewise, inclusion of dioctadecyldimethylammonium bromide (a cationic surfactant) into the formulation also led to large and size-uncontrolled particles. On the other hand, including 29% of water in the initial ethanolic solution leads to smaller particle sizes in the end, also in a controlled way also dependent on the flow rate ratio. In contrast, using a stabilizer to lipid ratio of 1:1 or 3:1 did not show a significant

change in the final sizes obtained. Altogether, these results suggest that cubosome size is directly dependent on the exchange rate of solvent molecules until a critical water concentration that induces particle formation is achieved. By allowing a precise control over the mixing and exchange between the two solvents, microfluidics promises to be a promising approach to further tailor the structure and efficiency of drug delivery systems. Nanoparticle size is a key parameter in the carriage of pharmaceuticals. Controlling cubosome size is therefore a relevant step towards the design of new and more efficient formulations.

Keywords

Cubosome; Microfluidic; Solvent Shifting; Solvent Exchange; Hydrodynamic Focusing; Mixing time; Size control; Self-Assembly

Contents

Index of abbreviations.....	XI
Index of figures.....	XIII
Index of tables.....	XXI
Aim	XXIII
Chapter 1 - General Introduction	1
1.1. Lipid-based systems	1
1.1.1. The hydrophobic effect and amphiphilicity drive self-assembly	2
1.1.2. Surfactant architecture dictates type of self-assembled structures	3
1.1.3. Other variables influencing self-assembly.....	7
1.1.4. The colloidal stability of dispersions.....	8
1.1.5. Cubosomes	10
1.2. Monoolein	11
1.2.1. Stabilizing cubic phase dispersions	13
1.2.2. Top-down approach synthesis	15
1.2.3. Bottom-up approach synthesis	15
1.2.4. State of art- Cubosomes and some technological applications.....	16
1.3. Microfluidics.....	17
1.3.1. Reynolds number.....	18
1.3.2. Péclet number	19
1.3.3. Mixing techniques.....	20
1.3.4. Active mixing techniques.....	21
1.3.5. Passive mixing techniques	21
1.3.6. State of art: Microfluidic devices for particle synthesis.....	23
Chapter 2 - Materials and Methods	26
2.1. Cubosome preparation using solvent-shifting in bulk:	26
2.2. Cubosome preparation using solvent shifting in a microfluidic device:.....	28
2.2.1. Preparation of Polydimethylsiloxane devices:	28

2.2.2.	Channel surface functionalization:	30
2.2.3.	Particle preparation using Solvent Shifting in a microfluidic device:	30
2.2.4.	Measurements of the focused stream:.....	32
2.3.	Characterization technique:	34
Chapter 3 - Results		39
3.1.	Formation of particles when co-flowing ethanol and water on a microfluidic device....	39
3.2.	Cubosome production using the solvent shifting technique	44
3.2.1.	Cubosome preparation: solvent shifting on bulk vs solvent shifting in microfluidics 45	
3.2.2.	Commercial cyclic olefin copolymer (COC) versus polydimethylsiloxane (PDMS)	51
3.2.3.	Influence of the stabilizer concentration and mixing ratio	54
3.2.4.	Increase in the lipid concentration.....	56
3.2.5.	DODAB:MO in liposome formation	59
Chapter 4 - Conclusion and future perspectives		61
Chapter 5 - Bibliography		63

Index of abbreviations

τ - Mixing time	22
D_R - Dilution ratio.....	28
H - Mean curvature.....	7
H_s - Spontaneous curvature.....	6
K - Gaussian curvature.....	7
L - Hydraulic diameter of the channel.....	20
l_{hc} - Length of the hydrophobic chain	4
P_e - Péclet number	22
Ps - Packing Parameter.....	3
Q_c - Flow rate of the centre stream	23
Q_R - Flow rate ratio	23
Q_s - Flow rate of a side stream.....	23
Q_t - Total flow rate.....	24
Re - Reynolds number.....	20
V_{hc} - Volume of the hydrophobic chain	4
w - Width of the focused stream.....	24
Z - Distance required in z axis to achieve mixing in a microfluidic device	22

Index of figures

Figure 1.1: Schematic drawing of a surfactant molecule. The surfactant molecules are divided into two groups, the polar/hydrophilic headgroup, and the apolar/hydrophobic.	2
Figure 1.2: Schematic drawing of a liposome. The liposomes are self-assembled structures used to encapsulate either hydrophobic drugs (■) in the hydrophobic region, or hydrophilic drugs (■) in the aqueous interior	2
Figure 1.3: The different main shapes that are present in the surfactants intrinsic nature and their corresponding packing parameters (P_s). For a packing parameter of 1, the format of the surfactant molecule is described as a cylinder whether for a P_s superior to 1/3 is of a cone or truncated cone and for a P_s superior to 1 the format is of an inversed cylinder.....	5
Figure 1.4: Structures formed according to the P_s of the surfactant molecule. Surfactant molecules with a P_s equal to 1 will favour bilayer structures, molecules with a P_s equal to 1/2 or 1/3 will favour cylindrical micelles and micelles and molecules with a P_s higher than 1 will favour inverted structures, respectively. The scale difference that these structures possess is also illustrated, demonstrating how does the size differ between a micelle to a regular bilayer.....	5
Figure 1.5: Curvature of the lipid films. For negative curvature values, an inverted structure is favoured; for a zero curvature, a planar structure is favoured; and for positive curvature values, a normal curvature is favoured.....	6
Figure 1.6: The many structures formed as a function of surfactant concentration and the packing parameter. The L_1 stands for the normal micelles, the I_1 for the various cubic micellar phases, the H_1 for the hexagonal phase, V_1 for the bicontinuous cubic phase $la3d$ and $Pn3m$, the V for the bicontinuous cubic phase $Im3m$, L_α for the lamellar phase, H_2 for the inverted hexagonal phase, the I_2 for the inverted micellar cubic phase and the L_2 for the inverted micellar phase. Reprinted with permission from ⁵	7
Figure 1.7: Schematic illustration of a DLVO potential between two colloidal particles dispersed in solution. The potential is composed by an attractive van der Waals force (blue) and a repulsive electrostatic force (red) components. The two potentials together result in long range repulsion and short range attraction, characterized by an energy barrier (or peak) that has to be overcome for the particles to aggregate. Once particles aggregate they reach a lower energy state making the aggregation irreversible. In the case of electrostatic forces, the addition of salt decreases its magnitude, lowering the energetic barrier for aggregation.	10

Figure 1.8: The three bicontinuous cubic phases. The Q_{II}^G (Ia3d) is the bicontinuous cubic Gyroid phase, the Q_{II}^D is the bicontinuous cubic Diamond phase and the Q_{II}^P is the bicontinuous cubic Primitive phase. Redrawn from ¹³ .	11
Figure 1.9: Schematic drawing of a monoolein molecule.	11
Figure 1.10: The monoolein-water phase diagram. L_c are presentations of a crystalline lamellar phase; L_α is the representation of the fluid lamellar phase; Q_{II}^G is represented by the inverted bicontinuous phase of the type Ia3d; Q_{II}^D is represented the inverted bicontinuous phase of the type Pn3m; L_2 represents the inverted micellar phase and H_{II} represent the inverted hexagonal phase. Until 60 wt% monoolein, it is possible to have liquid crystals dispersed in water, but above this concentration and depending on the temperature of system phase separation may occur. Redrawn from ¹⁵ .	12
Figure 1.11: Schematic illustration of the steric repulsive force due to a polymer coating. If the distance d between two surfaces becomes smaller than the coating thickness t the polymer chains overlap, reducing their conformational freedom and leading to a loss of entropy and repulsive force.	14
Figure 1.12: Ternary phase diagram of the monoolein:ethanol:water system at 25 °C. The diagram shows the existence of five single phase regions. An isotropic liquid phase (L_1), two bicontinuous cubic phases (Pn3m and Ia3d), one lamellar liquid-crystal phase (L_α) and what is thought to be a sponge phase (L_3). The start of the orange dashed arrow represents the initial composition of the lipid stock solution composed by monoolein:ethanol (1/99) that was used and, the tip of the arrow with the corresponding area (dashed line) represents the final concentration in each sample. The start of the blue arrow represents the initial composition of the lipid stock solution composed by monoolein:ethanol:water (1/70/29) that was used in the present work, and, the tip of the arrow with the corresponding area (dashed line) represents the final concentration in each sample produced using different flow conditions. The cubosome structures were observed by Spicer et al, at the two phase-region between the water apex and the left edge of the Pn3m region. Redrawn from ²⁹ .	16
Figure 1.13: Axial velocity flow profile inside a microchannel. The velocity U_z is independent of the position along the z axis, but it is dependent of the position in the y axis thanks to the no-slip boundary conditions. This means that the maximum velocity is in the centre of the channel and decreases as its position is closer to the walls of the microchannels.	19

Figure 1.14: Hydrodynamic focusing effects over the fluid streams. A) is a schematic top view of how the hydrodynamic focusing is visualized using a microscope. It can be noted that, the centre stream (→) is squeezed between two side fluids that come by the side inlets (↑↓). B) it's a schematic representation of the difference between stream width that is seen when using a microscope (grey dashed lines) and real focused stream width (blue lines). The view obtained is not of the focused width, but it is of the width of the focused stream at the microchannel walls. This width is significantly different than the focused one at the middle height of the microchannel, in the x axis. 23

Figure 2.1: Schematic representation on how to produce cubosomes using a solvent-shifting approach in bulk. The F127 solutions are put inside a vial that contains a stirring bar and is left for stirring for about 2 minutes. After that, a lipid stock solution is fiercely injected inside the vial and left for stirring for 2 extra minutes. At the end, the vial is recovered from the magnetic stirrer and the stirring bar recovered. 27

Figure 2.2: Picture of the setup made to produce cubosome particles using a microfluidic device with two syringe pumps and one microscope, to monitor the flow conditions. The inset represents a schematic view on the microfluidic device. Where the syringe 1, placed in the smallest syringe pump, contained the lipid stock solution and was connected to the centre inlet, while syringes 2 and 3 were placed together in the biggest syringe pump and contained the F127 solutions connected to the side inlets. Both three streams met at cross junction of the device, where the centre stream was hydrodynamically focused by the two side streams. After meeting at the cross junction, the three streams flowed together towards the outlet where they were collected at 4 (Eppendorf). 28

Figure 2.3: Schematic representation on, how to produce a PDMS microfluidic device. The process is divided into two phases, I and II. Phase I described the process in which the silica wafer is produced, with each number representing the order of the events, to work in phase II as a mould for the PDMS batch. The Phase II describes the process of producing the microfluidic device using the PDMS mixture with the cross linker (10:1). After mixing they are mixed with a spatula until it acquires a whitish aspect. The air bubbles are removed with the vacuum, at the dissecator, and then the object is put into the oven, at 65°C for at least 2 hours to cure the PDMS. The PDMS is then peeled off from the wafer, and the inlets are made with a plunger. With a clean glass slide, and with the PDMS cleaned, both are put under plasma treatment, to allow the irreversible linkage between them. 29

Figure 2.4: Schematic representation of the microfluidic hydrodynamic focusing approach used for controlled mixing and assembly of cubosomes of controlled size. In both setups (PDMS and COC) the microchannel width and height are ca. 100 μm . At such small cross-sections the flow tends to be laminar and mixing occurs by diffusion. By decreasing the width of the centred (focused) stream the distance that solvent molecules have to travel until mixing is achieved becomes smaller, leading to faster mixing times. The lipid stock solutions were injected in the centre inlet with flow rate Q_c , and the F127 solutions were injected in the side inlets, with flow rate Q_s . The solutions meet in the cross junction where the mixing process starts, with ethanol ($\uparrow\downarrow$) and water ($\uparrow\downarrow$) being mixed by diffusion while flowing towards the outlet, where the fluid was collected. Whereas ethanol is a good solvent for the lipids, water is not, favouring the formation of self-assembled structures. The rapid and controlled mixing of ethanol with water leads to the formation of cubosomes, whose size is controlled by manipulation of the speed of mixing. 32

Figure 2.5: Schematic representation of the cross section of an hydrodynamically focused stream, highlighting the concave flow profile (blue lines). The microscope observation takes as a reference the top wall of the device, and therefore, the measured width (in red) of the focused stream corresponds to its maximum width, giving an overestimation of the average width of the focused stream. 33

Figure 2.6: Graphical representation of a DLS measurement for larger particles (red) and smaller particles (blue). A) Light intensity profiles over time of smaller particles (top/blue) and smaller particles (bottom/red); B) autocorrelation function deducted from larger and smaller particles through different delay times. Redrawn from Hassan et al.⁶⁴. 35

Figure 2.7: DLS autocorrelation function ($G_2(\tau)-1$) data and fitting of a representative cubosome sample. A) The sample used was produced from a lipid stock solution of monoolein:ethanol (1/99) in a COC microfluidic device at a $Q_c=100 \mu\text{l}/\text{min}$ and $Q_s=10$. The measurements were performed at two different scattering angles (90° - circles, 173° - squares), and the data fitted with the cumulants method in a home-made Matlab routine, providing the characteristic decay constant Γ and polydispersity index (PDI). B) Fitting of the obtained Γ in A as a function of the scattering vector q^2 37

Figure 3.1: Optical Microscope images at the cross junction of the PDMS microfluidic device while injecting the solutions. Absolute ethanol was injected in the centre inlet and hydrodynamically focused at the cross junction by two side streams of water. In A) the hydrodynamically focusing enabled the formation of unexpected structures on the water sides, 1 minute after starting the

experiment. B) shows the formation and deposition of these unexpected structures as they grew 34 minutes after starting the experiment. The (→) are indications of the presence of unexpected structures..... 40

Figure 3.2: Optical microscope photograph from the cross junction of a microfluidic device, where absolute is squeezed by two water side streams. A) The ethanol stream is composed by ethanol at 82 wt% dissolved in water. B) The ethanol stream is composed by ethanol at 78 wt% dissolved in water. C) The ethanol stream is composed by ethanol at 76 wt% dissolved in water. The (→) are indicatives of the objects presence. 43

Figure 3.3: Optical microscope image at the cross junction of a PDMS microfluidic device while flowing ethanol at 76 wt% dissolved in water as the centre stream and water as the side streams. This device had at least five hours of continuous usage, and after this how structures we starting to form and precipitate at the microchannel walls, represented by the (→). 43

Figure 3.4: Average hydrodynamic diameter of particles formed by solvent shifting in bulk and using a COC microfluidic device. The dilution ratio (D_R) used for the preparation of the particles in bulk is equivalent to the flow rate ratio (Q_R) used to prepare the particles in the microfluidic device. Both (X) and (○) represent the average sizes for cubosomes prepared with solvent shifting in bulk. Where (X) is for cubosomes formed with a lipid stock solution of monoolein in absolute ethanol (1/99), and (○) represent the ones formed with a lipid stock solution of monoolein dissolved in an absolute ethanol:water mixture (1/70/29). The filled symbols (●) and (◆) represent the sizes of cubosome particles formed in the microfluidic chip, with (●) corresponding to particles obtained from a lipid:ethanol (1/99), and (◆) to particles obtained from a lipid:ethanol:water (1/70/29) stock solutions. Each data point corresponds to the average of at least two independently prepared samples. The solid lines represent fittings to the equation $D_h = A (D_R + 1)^2 + B$ (Eq. 36) with the fitting parameters A and B being 9300 and 140 for monoolein:ethanol, and 6500 and 100 for the monoolein:ethanol:water initial solutions, respectively. The dashed lines are guides to the eye. The excellent fit suggests the suitability of the model relating the cubosome size with the speed of mixing, controllable by D_R 46

Figure 3.5: Comparison between the focused width that is seen in a microscope during the hydrodynamic focusing inside a microfluidic device, and what is the typical width profile in a cross section inside the device. A) Photograph taken in the microscope during the hydrodynamic focusing inside the COC microfluidic device. B) Schematic representation of the cross section of an hydrodynamically focused stream, highlighting the concave flow profile (blue lines). The microscope

observation takes as a reference the top wall of the device, and therefore, the measured width (in red) of the focused stream corresponds to its maximum width, giving an overestimation of the average width of the focused stream. 50

Figure 3.6: Graphical representation of the focused ethanol stripe width (w_i), and its associated mixing time (τ), and channel length needed to achieve complete mixing (Z) as a function of D_r . Here $Q_i=100 \mu\text{L}/\text{min}$ (used in the COC device). In panel A, both (\blacktriangle) and (\blacktriangleleft) represent the measured w_i , and (\triangle) represents the estimated w_i using Eq. 28. In panels B and C, the mixing time τ is represented in the left ordinate axis whereas mixing length Z is represented in the right ordinate axis. Both (\blacksquare) and (\blacksquare) are a representation for τ and Z obtained using the measured w_i and calculated using the Eq. 26 and 27, while (\square) represents τ and Z using the estimated w_i . The orange symbols represent the data obtained when the lipid stock solution was composed by monoolein dissolved in absolute ethanol (1/99), and the blue symbols when it was dissolved in an absolute ethanol:water mixture (1/70/29). The three graphs show a decrease of both w_i , τ and Z , when D_r (and Q_r) is increased. Note however, that the measured widths and corresponding τ and Z are significantly overestimated due to the parabolic profile of the focused stream. 51

Figure 3.7: Average hydrodynamic diameter values and associated standard deviations for particles obtained using the PDMS microfluidic device (\bullet) and the COC microfluidic device (\blacklozenge) at different Q_r . The Q_i used in the PDMS microfluidic device was of $20 \mu\text{L}/\text{min}$ whether in the COC microfluidic device was of $100 \mu\text{L}/\text{min}$. The initial sample composition is (1/70/29) for lipid/ethanol/water wt%, and the lipid:F127 ratio is 1:1 for all Q_r . The size in both cases decreases as a function of Q_r . The sizes obtained using the COC device are smaller than the ones obtained in the PDMS device. This can be due to the different Q_i or due to the different surface properties of COC and PDMS. The solid lines represent fittings to the equation $D_h=A (D_r+1)^2+B$ (Eq. 36) with the fitting parameters A and B being 4900 and 123 for particles formed in the PDMS chip, and 5700 and 105 for particles formed using the COC microfluidic device, respectively. 53

Figure 3.8: Influence of the lipid:F127 mixing ratio on the average hydrodynamic diameters. The (\bullet) represent the average sizes of the particles produced with F127 side solutions at a constant mass ratio of 1 and the (\bullet) represent the ones produced with F127 side solutions at a constant mass ratio of 3. The size of the two types of particles created decreases as the Q_r increases without noticeable differences for the two lipid:F127 mass ratios. The solid lines represent fittings to the equation $D_h=A (D_r+1)^2+B$ (Eq. 36) with the fitting parameters A and B being 6000 and 125 for

particles formed using a F127:MO mass ratio of 3, and 4900 and 123 for particles formed at a F127:MO mass ratio of 1, respectively. 55

Figure 3.9: Influence of the lipid concentration on the average size of particles obtained using a COC microfluidic device at a Q of 100 $\mu\text{L}/\text{min}$. A) Average sizes of particles obtained from a lipid stock solution with Monoolein at 3 wt%. B) Average sizes of particles obtained from a lipid stock solution with Monoolein at 5 wt%. The orange symbols represent the data obtained when the lipid stock solution was composed by monoolein dissolved in absolute ethanol (1/99), and the blue symbols when it was dissolved in an absolute ethanol:water mixture (1/70/29). The solid lines represent fittings to the equation $D_p = A (D_0 + 1)^2 + B$ (Eq. 36) with the fitting parameters A and B of 13500 and 180 for monoolein:ethanol, and 2700 and 180 for the monoolein:ethanol:water initial solutions, respectively. The dashed lines are guides to the eye. The increase in lipid concentration leads to a poorer size control with microfluidics. At 3 wt% lipid some control over the size is still achieved..... 58

Figure 3.10: Microscope image of the COC device with strange structures precipitated inside the microchannels, when the flow of the centre lipid solution, of DODAB:MO (2:1) and side solutions of F127, was stopped. The presence of structures inside the microchannels are indicated by the blue arrows 60

Index of tables

Table 2.1: Volumes for mixing the lipid solutions, Monoolein with ethanol or Monoolein with ethanol:water mixture, with the F127 solutions to produce cubosomes with different batches of lipid solutions by the method described by Spicer et al. ²⁸ The solutions volumes are related with each Dilution factor that corresponds to a specific Flow Rate Ratio that was studied in the microfluidic devices.	27
Table 2.2: Flow rates used in each syringe pump to inject the solutions from the syringes to the microfluidic device for each of the Q_R used, at two different Q_C . The values for the Q_C sides are representative of the flow rates of the syringes that contain F127 solution and Q_C centre for the syringes that contain the lipid solutions.	31
Table 2.3: Calculated parameters for the estimated and measured focused width (w). The Eq. 9, 10 and 11 were used to calculate Pe , τ and Z the for all the Q_R at a Q_C of 100 $\mu\text{l}/\text{min}$. The measured focused centre stream width is used as an indication of the difference between what is measured in the microscope, and what is calculated using Eq. 16. This difference is explained in the in Figure 2.5.	34
Table 3.1: Solvent shifting in bulk results summary. The initial and final compositions of F127 aqueous solution and final lipid concentration were adjusted to span a D_R from 10 to 50 while keeping a constant lipid:F127 mass ratio of 1. The corresponding average sizes, standard deviations and PDI of the particles obtained when using initial solutions containing only lipid-ethanol and solutions containing lipid-ethanol-water are also shown.	45
Table 3.2: Solvent shifting results for the COC microfluidic device with constant final lipid:F127 mass ratio of 1. The particles obtained were from different lipid batches, one of monoolein 1 wt% dissolved in absolute ethanol and the other of monoolein dissolved in an absolute ethanol:water mixture (1/70/29). The average size and associated standard deviation, as well as PDI were always smaller for particles where the lipid stock solution contained water.	48
Table 3.3: Comparison of the size parameters of particles prepared using a PDMS and a COC microfluidic device. Particles produced in the COC microfluidic device are smaller and show smaller standard deviation. The initial lipid solution has a composition of 1/70/29 lipid/ethanol/water wt%.	53
.Table 3.4: Solvent shifting results for an initial monoolein concentration of 3 wt%. The final lipid:F127 mass ratio is 2 and kept constant for the different Q_R . The used microfluidic device is	

the COC. The particles obtained were from different lipid batches, one of monoolein 3 wt% dissolved in absolute ethanol and the other of monoolein dissolved in an absolute ethanol:water mixture (3/70/27). At these higher initial lipid concentrations the size standard deviation and PDI increases. Again, similarly to the more dilute lipid cases, the average size, size standard deviation, and PDI were smaller for particles where the lipid stock solution contained water. 57

Table 3.5: Solvent shifting results for an initial monoolein concentration of 5 wt%. The final lipid:F127 mass ratio is 2 and kept constant for the different Q_R . The used microfluidic device is the COC. The particles obtained were from different lipid batches, one of monoolein 5 wt% dissolved in absolute ethanol and the other of monoolein dissolved in an absolute ethanol:water mixture (5/70/25). At such high initial lipid concentrations the production of the cubosome particles seems to become uncontrolled, leading to erratic trends in the sizes. 57

Table 3.6: Average sizes with associated standard deviation, and PDI for the particles formed in a COC microfluidic device at different Q_R . Both and PDI were indicating that the results were a consequence of the loss of control over the particles that were being formed. 60

Aim

The main aim of this work is to produce cubosomes with tuneable sizes using microfluidic devices with hydrodynamic focusing. Special emphasis is put on the tuning of the cubosome size just by manipulation of the flow conditions inside the microfluidic chip. A secondary goal is to investigate the influence of the compositional parameters of the initial and final solutions, i.e. lipid composition, amount of stabilizer, total lipid concentration and water/ethanol concentration. A third goal implied the usability of polydimethylsiloxane (PDMS) and cyclic olefin copolymer (COC) as valid materials for the microfluidic chips.

Chapter 1 - General Introduction

Every year new drugs are developed with many showing promising results in vitro studies.¹ However, their application in human patients often fails. This failure can be the result of many factors, such as poor solubility, low bioavailability, short blood circulation half-times and the lack of targeting to the specific target area. This inefficiency often forces the use of higher dosages in therapies that lead to strong and undesired side effects.^{2,3}

To overcome these difficulties, drug delivery systems are continuously being developed, bringing new therapy opportunities to the pharmacy industry. These systems, can explore the use of different routes of administration since they permit the shielding of the drug molecules from the biological environment, which not only hinders these molecules to non-specific binding with unspecific proteins, but it also protects other tissues from the action of these drugs. Another important feature provided by these systems is the ability to target the site of action of these molecules while allowing their controlled leakage from the carriers.

1.1. Lipid-based systems

Lipid nanocarriers are some of the most used drug delivery systems. These systems are mainly constituted by amphiphilic lipid molecules. Being amphiphilic means that such lipid molecules are constituted by two different domains of very different polarities and affinity towards water: the hydrophobic domain (i.e. the tail), composed by one or more hydrocarbon chains; and a hydrophilic domain (i.e. the headgroup) – Figure 1.1. As will be seen below, it is this amphiphilicity that drives the self-assembly of lipids into a broad range of structures that can be used to encapsulate poorly-water soluble drugs in their interior (Figure 1.2). Another important aspect behind the widespread use of lipids over other type of nanocarriers is the biomimetic properties of the lipid membranes, which lead to significantly lower toxicities when compared with other systems.

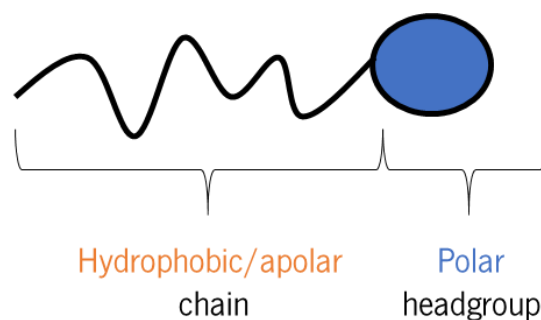


Figure 1.1: Schematic drawing of a surfactant molecule. The surfactant molecules are divided into two groups, the polar/hydrophilic headgroup, and the apolar/hydrophobic.

The surfactants used to produce lipid assemblies are usually classified according to their charge (anionic, cationic, zwitterionic, catanionic, non-ionic), or to their architecture (number of chains, number and placement of the headgroups such as in bolaamphiphilic and gemini surfactants, etc). All this diversity gives rise to a richness of self-assembly behaviour that can be explored to design the most suitable lipid particle for a given application.

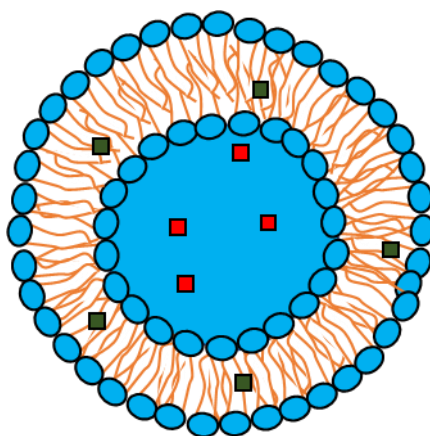


Figure 1.2: Schematic drawing of a liposome. The liposomes are self-assembled structures used to encapsulate either hydrophobic drugs (■) in the hydrophobic region, or hydrophilic drugs (■) in the aqueous interior

1.1.1. The hydrophobic effect and amphiphilicity drive self-assembly

The process in which the lipid nanoparticles are formed is called self-assembly. The process itself is the result of the hydrophobic effect, a free energy penalty that is associated with the unfavourable interactions between the hydrocarbon chains and the water. These interactions force the water molecules to form very organized networks (known as clathrates) around the hydrocarbon chains. The formation of these clathrates around the alkyl tails leads to a decrease in

the entropy, which results in a free energy penalty when solubilizing lipid/surfactant molecules in solution.⁴ These unfavourable interactions between the alkyl tails and water thus drives the formation of self-assembled structures, where the hydrocarbon chains are located in the core of the aggregates (to reduce contact with water molecules), and the headgroups are located at the interface. On the other hand, the formation of the aggregates brings the polar headgroups together, which brings also a free energy penalty (for instance, ionic headgroups have unfavourable electrostatic interactions amongst themselves). The optimal balance between the hydrophobic effect, that tries to place the alkyl tails together, and repulsions between headgroups that tries to put them apart drives the self-assembly into a rich variety of structures, depending on the surfactant intrinsic properties and environment conditions. The most common arrangements have micelles and bilayers as unit structures.

1.1.2. Surfactant architecture dictates type of self-assembled structures

When assembling the surfactant molecules, there is a rich variety of structures that can be obtained. These structures can range from micelles to bilayers and other structures, depending on the lipid molecule's physical properties. As seen above, self-assembly into micelles, bilayers, and other structures is the result of a balance between the hydrophobic effect, that enables the self-assembly process, and the repulsion forces that arise from the interaction between the headgroups of each monomer.⁵ The structures formed, when dispersing the surfactant molecules into an aqueous medium, depend on more than one factor, but the leading parameter influencing the type of self-assembly observed is the architecture of the surfactant, including the nature of the headgroup (ionic, non-ionic, etc).

The packing parameter (P_s) can be used to predict what type of structure will be formed based on the surfactant molecule shape. It consists on the ratio of hydrophobic volume to hydrophilic area, i.e. the volume occupied by the hydrocarbon chains to the headgroup area.

The P_s is written as follows,

$$P_s = \frac{V_{hc}}{l_{hc}a_{hg}} \quad 1$$

where V_{hc} is the hydrocarbon chain(s) volume, the l_{hc} is the hydrocarbon chain length and the a_{hg} the headgroup area.

To calculate the volume and length of the hydrophobic chain, a fully extended saturated chain is assumed, which depends directly on the number of carbons (nc),

$$V_{hc}/nm^3 = 0.0274 + 0.0269nc \quad 2$$

$$l_{hc}/nm = 0.154 + 0.127nc \quad 3$$

where 0.0269 is the volume of a non-terminal methyl group and 0.0274 nm³ is the volume of the terminal methyl group. Likewise, 0.154 nm is the Van der Waals radius of the terminal methyl group and 0.127 nm is the bond length between two carbons.⁴

The calculation of the polar headgroup area is significantly more complicated due to all the interactions that occur between the headgroup and its surroundings. If considering an ionic surfactant, the headgroups will in principle have the same charge, which leads to a repulsive force that makes the effective area of the headgroup larger than its physical area if the group was uncharged.

Due to these difficulties, an accurate calculation of the P_s is difficult, but this still a powerful qualitative way of predicting the phase behaviour of lipid and surfactant systems. For instance, based on these qualitative assumptions, one can expect that addition of salt to a micellar system composed of ionic micelles leads to a decrease of the effective headgroup area, and thus to an increase of P_s . This is indeed the case for systems such as DTAB or CTAB, where the addition of salt leads to a micellar growth from spherical to worm-like micelles.⁶

To better understand the dynamics in which P_s is used, one can consider a cylinder format, where the headgroup area is the area of one of the two faces in the cylinder and the hydrocarbon chains represent its length. As the area of the headgroup is getting bigger, the molecule will have a cone shape format, however if the headgroup area is getting smaller than the format obtained will be like an inverted cone shape, Figure 1.3

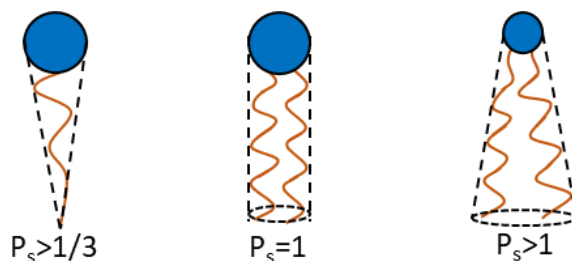


Figure 1.3: The different main shapes that are present in the surfactants intrinsic nature and their corresponding packing parameters (P_s). For a packing parameter of 1, the format of the surfactant molecule is described as a cylinder whether for a P_s superior to $1/3$ is of a cone or truncated cone and for a P_s superior to 1 the format is of an inversed cylinder.

The shapes described by the P_s are indicative of the types of aggregates formed, and these can be thought as an optimal way of packing the surfactant molecules whose shapes are approximated by the geometrical objects described by P_s . If the shape that is present is of a cylinder, the preferred structure will be of bilayer with mean zero curvature. If the shape is closer to a cone, than the preferred structures will mainly be of micelles. The opposite is expected if an inverted cone shape is present, here the volume of the hydrophobic part is significantly bigger than the hydrophilic area of the headgroup and so, the favoured structures will be of inverted nature with negative curvatures (Figure 1.4).

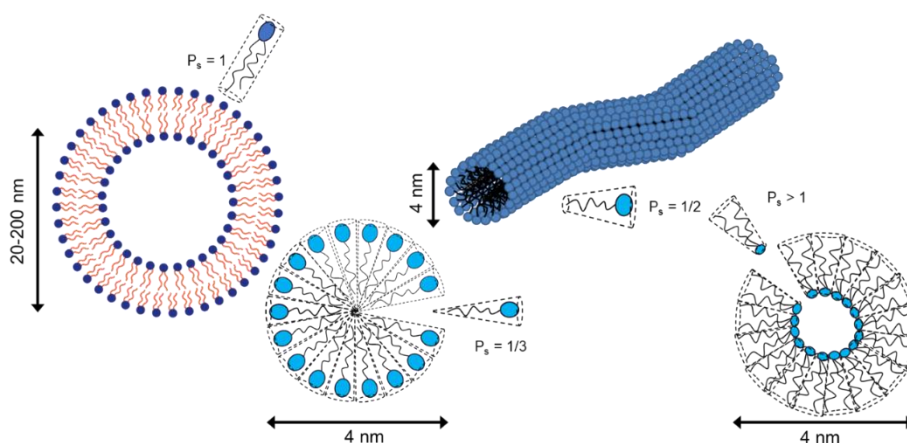


Figure 1.4: Structures formed according to the P_s of the surfactant molecule. Surfactant molecules with a P_s equal to 1 will favour bilayer structures, molecules with a P_s equal to $1/2$ or $1/3$ will favour cylindrical micelles and micelles and molecules with a P_s higher than 1 will favour inverted structures, respectively. The scale difference that these structures possess is also illustrated, demonstrating how does the size differ between a micelle to a regular bilayer.

The spontaneous curvature (H_0) similarly to the packing parameter, can also be used for predicting what kind of structure will be obtained. Both rely on the same principle, the hydrophobic volume to the hydrophilic area, but they differ on a simple point, in a packing parameter assumption the entity that is considered is a surfactant molecule whether in the spontaneous curvature, the surfactant film as a whole is considered as one entity.

The H_0 is the surface spontaneous mean curvature that an aggregate possesses when no external input is being considered, like any kind of mechanical or chemical stress. It is written as,

$$H_0 = \frac{1}{2} \left(\frac{1}{R_1} + \frac{1}{R_2} \right) \quad 4$$

where R_1 and R_2 are two perpendicular radii.

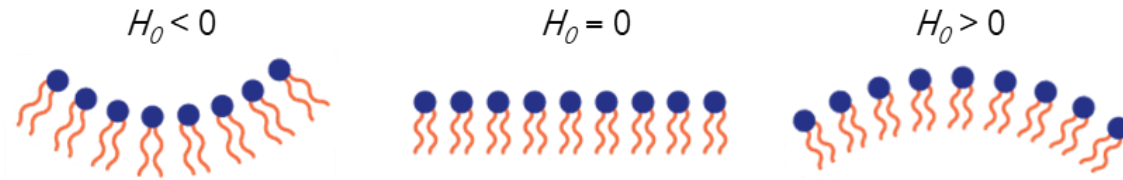


Figure 1.5: Curvature of the lipid films. For negative curvature values, an inverted structure is favoured; for a zero curvature, a planar structure is favoured; and for positive curvature values, a normal curvature is favoured.

If the R_1 and R_2 are finite and have the same value, the expected surface obtained is of a sphere, but if one of the R is finite and the other is infinite then a cylinder shape is favoured. To have a planar shape, the H_0 must be zero and both R values have to be infinite. There is another possibility to obtain a H_0 of zero as will be described below.

First let us introduce the local curvature free energy g , which to first order can be described by:

$$g_c = 2k (H - H_0)^2 + \bar{k}K \quad 5$$

Here, H is the mean curvature (equivalent to H_0 but not the equilibrium curvature), K is the Gaussian curvature, and k and \bar{k} are the bending and saddle splay moduli, respectively. The Gaussian curvature K is defined as:

$$K = \frac{1}{R_1 R_2} \quad 6$$

The curvature free energy g shows that bending the mean curvature out of its equilibrium value has an energy penalty proportional to the bending modulus and the square of the difference

between H and \bar{K} . It also shows that if \bar{K} is positive, then g decreases if the K becomes negative. In order for K to become negative, the two radii R_1 and R_2 have to be finite but of opposite signs. Hence, if R_1 and R_2 are equal in magnitude but opposite in sign, K is negative while H is zero.

This is the case for bicontinuous cubic phases. For such systems the saddle splay modulus is positive leading to the formation of bicontinuous cubic systems to satisfy a negative Gaussian curvature and mean curvature of zero.

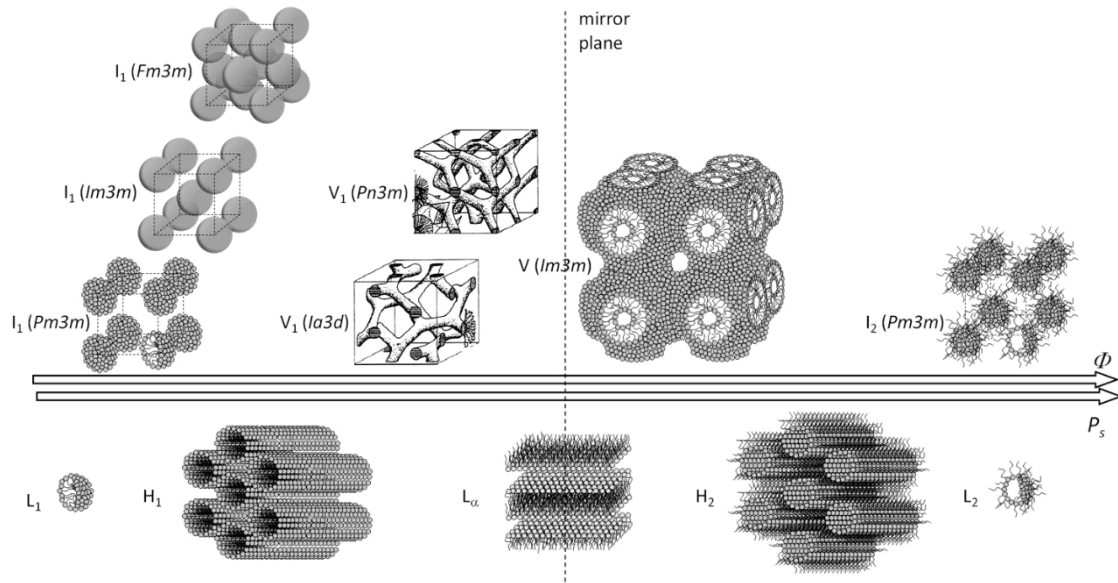


Figure 1.6: The many structures formed as a function of surfactant concentration and the packing parameter. The L_1 stands for the normal micelles, the I_1 for the various cubic micellar phases, the H_1 for the hexagonal phase, V_1 for the bicontinuous cubic phase $Ia3d$ and $Pn3m$, the V for the bicontinuous cubic phase $Im3m$, L_α for the lamellar phase, H_2 for the inverted hexagonal phase, the I_2 for the inverted micellar cubic phase and the L_2 for the inverted micellar phase. Reprinted with permission from⁵.

A more detailed look into these aspects can tell us that, the bending modulus (k) is a representation of the difficulty to bend the film and, the Gaussian curvature modulus (\bar{K}) of its topology.^{4,5}

The P_s , H_0 , K , k and \bar{K} result firstly from the intrinsic properties of the surfactant that is being used but other external variables also need to be considered as shown below.

1.1.3. Other variables influencing self-assembly

As mentioned above, the architecture of the lipid molecules, embodied through the P_s parameter, has a crucial role in determining the self-assembled structures to be formed. However,

other parameters, such as surfactant concentration, temperature, ionic strength and other additives (e.g. oil, alcohol and co-surfactant) also influence the structures formed.

Among the many subjects used, salt, co-surfactants, surfactant concentration, temperature, type of oil and ionic surfactants of opposite charge, are the most relevant.

If the surfactant used is of ionic nature, then with an increase in salt concentration in the solution it is possible to screen its charges around the aggregate surface, this screening enables a curvature transition from positive-to-negative, depending on the surfactants used. Something similar happens when a surfactant of opposite charge is added, the surfactants with opposite charge diminish the repulsive electrostatic interaction among them and so, the hydrophilic area occupied by their headgroups is diminished leading to larger P_s and smaller H .⁴

The oil insertion can alter the curvature, as the oil is being added it moves to the aggregates core increasing the hydrophobic volume and so, an inversion of curvature from negative-to-positive is possible.⁴

Temperature has an opposite effect for ionic surfactants and non-ionic surfactants of the C_nE_m type (in which m indicates the number of alkyl groups in the tail and n indicates the number of polyethylene oxide units in the headgroup). If considering non-ionic C_nE_m surfactants, the increase of temperature leads to a decrease in the solvent shell around the headgroups of the surfactant molecules, this decrease is translated in the decrease of the a_{hg} which in turn makes the P_s bigger and H smaller. If considering the ionic surfactants, the change in temperature has a weak effect on the aggregates. Part of the temperature effect is located at the hydrocarbon chains where the number of gauche conformations is increased with the temperature – this decreases H . However, the electrostatic Gibbs free energy, which is mainly entropic, is also increased leading to an increase in H . The resulting effect is a slight increase in the H for ionic surfactants.⁴

The surfactant concentration is another way to affect the aggregates structure. It is related with the amount of water volume that is available. With the increase in surfactants concentration, the number of aggregates is also increased, and this leads to less space in the water medium which results in more interactions between the aggregates, these interactions may result in posterior structural changes in order to fit all the aggregates in the available space.⁴

1.1.4. The colloidal stability of dispersions

In homogeneous systems (one phase systems), micellar solutions are present at dilute and semi-dilute lipid concentrations. They can be either normal or inverted, and are classified as

isotropic phases since they do not possess long range positional nor orientational order, i.e. the solution is structurally homogenous in the three spatial dimensions.⁷ One important aspect of isotropic solutions such as micelles is that besides one being able to distinguish the medium from the aggregates, these two components are part of the same phase since this represents a thermodynamic equilibrium and a true minimum in energy. That is, in a micellar phase, the formation of micelles in solution represents the most energetically favourable way to arrange all the molecules in solution, and therefore the solution and structural properties do not change with time. This is fundamentally different from colloidal dispersions, in which one phase like oil is dispersed in another phase like water. In such cases, the equilibrium state tends to be complete phase separation of oil and water, since the energy can be minimized in such way. However, in order for such dispersions to aggregate or coalesce, they have energy barriers that have to be overcome. If the energy barrier opposing fusion of two oil droplets in water (e.g. if the oil droplets are sterically stabilized by a surfactant or polymer) is large, these dispersions can be stable for long periods of time, and make the dispersions useful for practical applications. Yet, over long periods of time these dispersions can become unstable.

A theoretical framework useful for the understanding of colloidal stability is the DLVO theory (after the physicists Derjaguin, Landau, Verwey and Overbeek), which considers the van der Waals force (that is always attractive) but short-ranged, and the electrostatic repulsion, which is repulsive and more long ranged. At long distances the electrostatic force dominates and the dispersed particles have a net-repulsive interaction. However, if they come closer than a critical distance, the van der Waals force which is stronger at smaller distances starts to dominate and induce a net-attractive force which pulls the particles together destabilizing the solution (Figure 1.7).

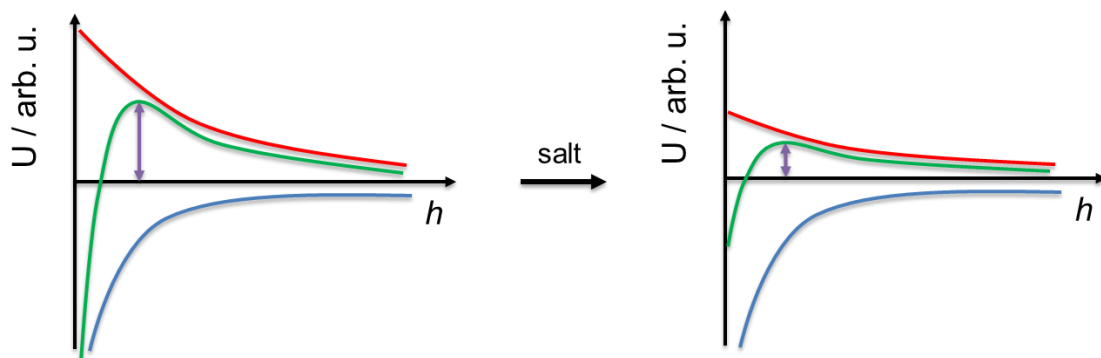


Figure 1.7: Schematic illustration of a DLVO potential between two colloidal particles dispersed in solution. The potential is composed by an attractive van der Waals force (blue) and a repulsive electrostatic force (red) components. The two potentials together result in long range repulsion and short range attraction, characterized by an energy barrier (or peak) that has to be overcome for the particles to aggregate. Once particles aggregate they reach a lower energy state making the aggregation irreversible. In the case of electrostatic forces, the addition of salt decreases its magnitude, lowering the energetic barrier for aggregation.

The relevance of this topic asserts in the fact that cubosomes constitute dispersions of a bicontinuous cubic stabilized by a block copolymer in excess solvent. Hence it is a two-phase system that has some kinetic stability due to the action of the polymer stabilizer, but with time can aggregate back to a macroscopic phase separation of the bicontinuous cubic phase plus excess water. For this reason, surface chemistry plays an important role on colloidal stabilization, and will be addressed in the next sections⁹

1.1.5. Cubosomes

Cubosomes were first introduced and described by Kåre Larson in 1989⁹. Cubosomes are nano-sized lipid-based dispersions of bicontinuous cubic phases in excess water, and typically stabilized by an amphiphilic polymer. These particles phases are described as bilayers periodically curved in three dimensions, which result in a hydrophobic matrix with non-intersecting water channels.¹⁰ These features are of particular interest when trying to encapsulate other molecules, since the structure itself possesses both hydrophobic and hydrophilic domains along with the interface between both.^{11,12}

The bicontinuous phases are described by possessing mean surface curvatures of 0, where the gaussian curvature assumes negative values or increasing values towards zero depending on the surface position. They can be thought as saddle points, where the curvature at each point is cancelled by opposite radius. The cubic phases can be divided into three main types:

the gyroid (G) phase (from the Ia3d space group) which is described by possessing interconnected channels 3-by-3 separated by a G-minimal surface; the diamond (D) phase (from the Pn3m space group) that is composed by interconnected water channels 4-by-4 separated by a F-minimal surface; and the primitive (P) phase (from the Im3m space group) that is composed by interconnected water channels connected 6-by-6 and separated by a P-minimal surface.¹³

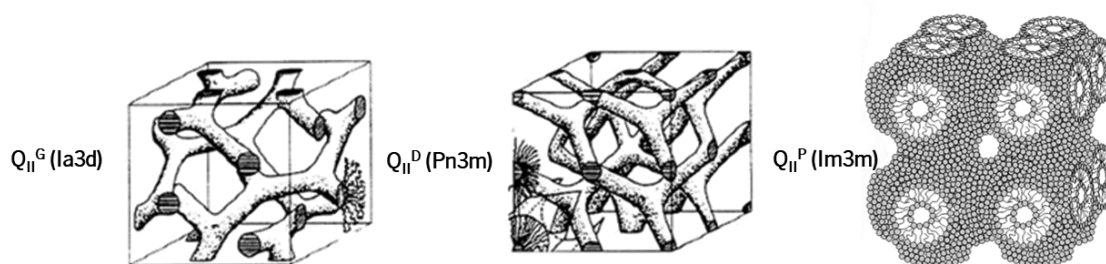


Figure 1.8: The three bicontinuous cubic phases. The Q_{II}^G (Ia3d) is the bicontinuous cubic Gyroid phase, the Q_{II}^D is the bicontinuous cubic Diamond phase and the Q_{II}^P is the bicontinuous cubic Primitive phase. Redrawn from¹³.

Cubosome particles offer unique properties when comparing with their counterparts as an encapsulating agent and among them, the increased inner surface area and the hardness present in these systems seem the most distinguishable.¹⁴

1.2. Monoolein

Glyceryl monooleate, 1-monoolein or just monoolein (MO), is an amphiphilic molecule constituted by one hydrocarbon chain (tail) that is connected to a glycerol backbone (headgroup) by an ester bond. At the glycerol backbone, two carbons show active hydroxyl groups that confer polarity to this unity of the molecule. A double *cis* bond can be found at the 9th-10th position of the hydrocarbon chain, which provides the characteristic kink in the arrangement of the tail, Figure 1.9.^{15,16}



Figure 1.9: Schematic drawing of a monoolein molecule.

Monoolein use started as an emulsifying agent and as a food additive back in the 50s, but since 1984 it gained an increased importance when it was proposed as a biocompatible encapsulating agent with controlled release. Since then, it was associated with cosmetics, food and pharmaceutical formulations.¹⁶⁻¹⁹

This increased interest in monoolein, a rather simple molecule, also comes from the fact that it can assemble to form various liquid crystalline structures. These structures can be formed according to the way the molecules assemble when changing the temperature or water content, allowing the formation of the so called thermotropic and lyotropic phases, respectively.¹⁵ It is generally assumed that, with a decrease in the water content the formation of well-defined structures are promoted.²⁰

To better understand the liquid crystals that are formed using monoolein and water, the monoolein-water phase diagram is used, Figure 1.10. This diagram is the reflection of what type of structures are formed as a function of temperature and water content on the system, when the system is at thermodynamic equilibrium, i.e. at its lowest state of free energy.¹⁵

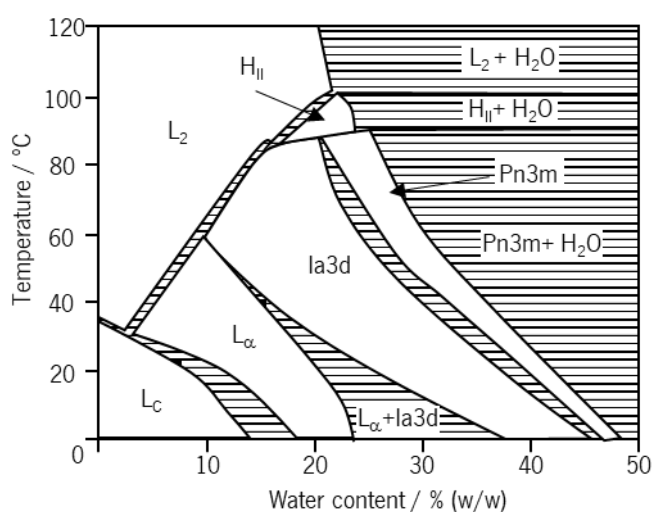


Figure 1.10: The monoolein-water phase diagram. L_c are presentations of a crystalline lamellar phase; L_α is the representation of the fluid lamellar phase; $Ia3d$ is represented by the inverted bicontinuous phase of the type $Ia3d$; $Pn3m$ is represented the inverted bicontinuous phase of the type $Pn3m$; L_2 represents the inverted micellar phase and H_{II} represent the inverted hexagonal phase. Until 60 wt% monoolein, it is possible to have liquid crystals dispersed in water, but above this concentration and depending on the temperature of system phase separation may occur. Redrawn from¹⁵.

Monoolein has a tendency to form structures with mean spontaneous curvature of zero and negative Gaussian curvature. This can be best understood by looking at the $Pn3m$ plus water two-phase region near room temperature. In this case, there is enough water for the system to

form other types of structures, but the most favourable configuration is for monoolein to form a bicontinuous cubic phase of the Pn3m type, incorporating ca. 42 wt% water, and letting the remainder water in excess outside. At water contents below, the water channels inside the bicontinuous structure start narrowing down, but close to ca. 40 wt% the system separates into two bicontinuous cubic phases – the Pn3m and the Ia3d phase – and at ca. 37 wt% the system enters in a single Ia3d phase. This suggests at lower water amounts the Ia3d phase can accommodate better the available water in its water network. At even lower water contents, the Ia3d phase is not stable either (there is not enough water to sustain the water network), and the system prefers a lamellar phase with small amounts of water between the bilayers.

On the other hand, by choosing a fixed water composition and increasing the temperature, one can realize that the curvature is becoming increasingly negative. If one departs from within the Pn3m one-phase region and increases de temperature will reach a point where water starts to phase-separate. This suggests that by becoming more negative, the surfactant film narrows down the water channels expelling water. Likewise, at higher temperatures an inverse hexagonal phase, whose curvature is more negative, is also found.¹⁵

1.2.1. Stabilizing cubic phase dispersions

The monoolein dispersed phases are not stable in water, in fact they are metastable, which is state with some transient stability but not truly a state of minimum energy in the overall system. As the time passes, these structures tend to aggregate to minimize the free energy of the system. They can aggregate by different mechanisms like the Ostwald Ripening effect, sedimentation, flocculation or coalescence.⁷ By aggregating, phase separation between lipid-to-water occurs. In technological applications it is often desired to keep these dispersed phases as stable as possible and prevent aggregation.

To difficult the transition between a dispersed system to a phase separated one, the energy barrier required for the phase separation must increase. The use of stabilizers in dispersions, can significantly increase this barrier by providing repulsive interactions between molecules, as seen before in. Figure 1.7 In some cases, stabilized particles like this can be very stable over time, but most often they tend to eventually aggregate after some time that can go from hours to years. These repulsive interactions can be either electrostatic or steric. However, it is important to note that the use of these stabilizer molecules can also interfere in the particles internal structure, being capable of smooth to drastic changes.^{21,22}

The steric repulsive interactions are the ones present when using a non-ionic polymer to coat the dispersed particles. These interactions are increased as the distance between two separated aggregates undergo smaller distances than twice of the thickness of the coating (Figure 1.11). If the distance between two particles becomes smaller than twice the coating thickness, the polymers start to overlap, which leads to a loss of entropy, and therefore a repulsive force of steric origin is felt that stabilizes the particles.⁴

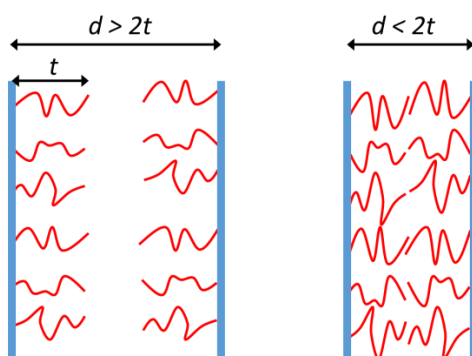


Figure 1.11: Schematic illustration of the steric repulsive force due to a polymer coating. If the distance d between two surfaces becomes smaller than the coating thickness t the polymer chains overlap, reducing their conformational freedom and leading to a loss of entropy and repulsive force.

Poloxamer 403, or commonly known as F127, is a tri-block non-ionic copolymer composed by one hydrophobic group intercalated in the middle of two hydrophilic groups and, is the most employed stabilizer for lyotropic cubic phases. Its hydrophobic group is composed by an average of sixty-five units of polypropylene oxide (PPO) and the hydrophilic groups are composed by an average of one hundred units of polyethylene glycol (PEG).^{23,24}

Nakano et al. (2001)²⁵ showed that, when using F127 within the monoolein/water system, the F127 molecules seem to adsorb at the cubosomes surface if used at less than 3 wt%. At this amount, the bicontinuous phase present is the Pn3m but, at increased amounts of F127, the Im3m is promoted, meaning that the F127 can affect the internal structure of the monoolein system since this phase was not detected if F127 was not used. Also, the use of F127:MO at weight ratios up to 10% promotes a decrease in the cubosomes size, whilst above this ratio the size is stationary.

When possessing a given formulation to produce the particles, two approaches can be made to synthesise them, a top-down approach and a bottom-up approach.

1.2.2. Top-down approach synthesis

The top-down synthesis consists on using a suitable starting material, and then with high energetic inputs, break the material into smaller fragments to form the desired structures. This approach is performed with high-pressure homogenization and sonication techniques.²⁶⁻²⁸ These techniques are often referred as damage promoters on the amphiphilic structures thanks to the resulting increased temperature.

Although there are a few advantages associated with the use of these systems, the disadvantages are the ones that make them unsuitable for large scale production. The need to previously form a very viscous cubic structure (starting material), demands a high amount of energy that can limit the incorporation of some temperature sensitive molecules. Also, the existence of unwanted vesicles is also often detected.^{10,24,29,30}

1.2.3. Bottom-up approach synthesis

The bottom-up synthesis works in the opposite way of the top-down technique, i.e. small building block units are dispersed in an aqueous medium to form the final functional material. Solvent shifting (or solvent exchange) is a bottom up approach that consists in solubilizing the lipids in a solvent that is miscible in water (typically ethanol) in a first step. After, the precursor solution is quickly injected in water, where the solvent exchange leads to the nano-precipitation or self-assembly of the lipid molecules into the desired structures.³¹

The advantages in this method can range from the low energy requirement for particle synthesis which enables the use of temperature sensitive molecules, to the smaller and more stable cubosomes obtained when compared with a top-down approach. Still, there are some disadvantages when using this process. The water miscible solvents are usually toxic to the human body and the existence of additional structures can be also found. Finally, a profound knowledge on the ternary phase diagram of the lipid, water, and water-miscible solvent system is required.^{10,24,29,30}

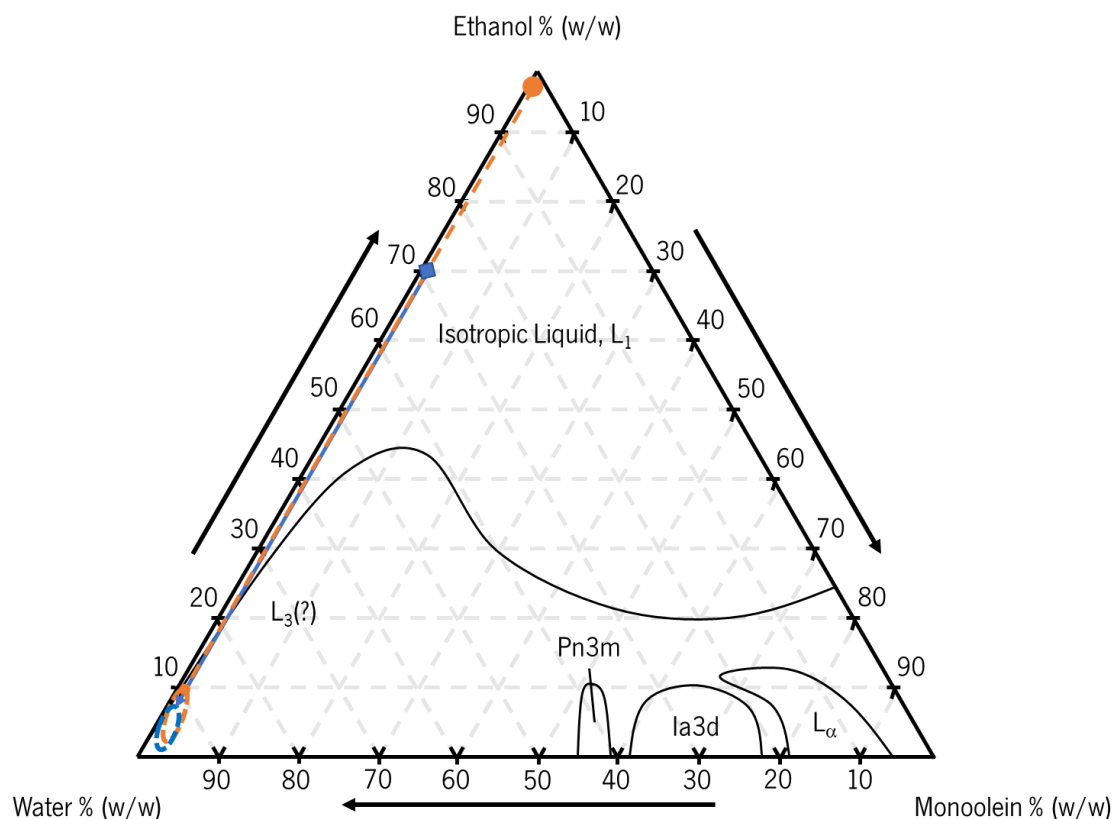


Figure 1.12: Ternary phase diagram of the monoolein:ethanol:water system at 25 °C. The diagram shows the existence of five single phase regions. An isotropic liquid phase (L_1), two bicontinuous cubic phases (Pn3m and Ia3d), one lamellar liquid-crystal phase (L_α) and what is thought to be a sponge phase (L_3). The start of the orange dashed arrow represents the initial composition of the lipid stock solution composed by monoolein:ethanol (1/99) that was used and, the tip of the arrow with the corresponding area (dashed line) represents the final concentration in each sample. The start of the blue arrow represents the initial composition of the lipid stock solution composed by monoolein:ethanol:water (1/70/29) that was used in the present work, and, the tip of the arrow with the corresponding area (dashed line) represents the final concentration in each sample produced using different flow conditions. The cubosome structures were observed by Spicer et al, at the two phase-region between the water apex and the left edge of the Pn3m region. Redrawn from³¹.

Figure 1.12 represents the phase diagram of the monoolein:ethanol:water system. The diagram exhibits the presence of five single phase regions. Two of those regions are bicontinuous cubic phases, namely the Pn3m and the Ia3d. The cubosome region was found, by Spicer et al. (2001)³¹ to be from the water apex to the top and bottom left edge of the Pn3m phase region.

1.2.4. State of art- Cubosomes and some technological applications

Dispersed bicontinuous cubic phases or just cubosomes, since their first description by Larson (1989)⁹ and, their imaging by Gustafsson et al.(1996),¹¹ have been gaining considerable

interest, being described as excellent encapsulating agents, with both hydrophilic and hydrophobic domains, and above that, high surface to volume ratio.

Monoolein is a lipid molecule that forms these so-called cubosomes, and although only water is required to form these structures, with time they tend to aggregate which means that they require the use of a stabilizer. Nakano et al.(2002)³² studied the influence of F127, a co-polymer that could work as stabilizer, on the cubosome formation using monoolein. He demonstrated that an increase in polymer concentration could indeed decrease the cubosomes size and suggested that the polymer was placed on the cubosome surface. Chong et al. (2011)³³ investigated the use of new stabilizers to replace F127, and were able to demonstrate that Pluronic F108 was more effective than F127, since it preserved the internal structure of the cubosome while maintaining its colloidal stability.

In 2010 Guillot et al. (2010)³⁴ demonstrated the influence of the stabilizer concentration on monoolein loaded cubosomes, they found out that an increase in the concentration of the stabilizer could truly force a phase transition in the internal structure of the cubosomes.

The use of different types of stabilizers were analysed by Chong et al.(2014)²³ They showed that brush type co-polymers provided a more effective stabilization of the particles when compared to linear types, like F127.

The internal cubosome structures is of main interest, and a few studies concerning the ability to change these structures indicated that pH can induce phase transitions in dioleoylphosphatidylserine/monoolein membranes. Also, the use of unsaturated fatty acids have been linked as promoters for phase transitions.^{35,36}

Studies have also demonstrated that cubosomes can offer a control and sustained release of the active molecules.²⁰

1.3. Microfluidics

The microfluidic technology is described as the manipulation of small amounts of fluids at the micrometre scale. To do so, these systems are usually composed by channels with micrometre dimensions, which enable the fluid streams to operate at low Reynolds numbers, as will be briefly discussed below.^{37,38}

The technology itself began its pathway in the analysis field, although its scope was the integration in MEMS systems, the use of capillaries revolutionized the existent analysis techniques.³⁷ Microfluidics is now a technology that is being applied in almost every research area, from the lab

on chip concepts (where is intended to join synthesis, analysis and reactions), to sensors, actuators and analytical chemistry using small volume of reagents.³⁹

Microfluidic techniques have also been used in the formation of nanoparticles to improve the otherwise poor control over the particles synthesis when using the more conventional bulk techniques. Such bulk methods typically do not allow a controlled distribution of molecules leading to uncontrolled and dispersed sizes of the particles.^{10,40,41}

The size control is a very important feature in the drug delivery technology, because as the size is increased, the faster those particles are cleared from blood circulation, making the technology inefficient from its very start.⁴²

1.3.1. Reynolds number

Microfluidic devices usually operate under low Reynolds numbers. Which enables the control of the mixing and fluid dynamics in the desired lengths. The Reynolds number is a dimensionless number used to characterize the ratio between inertial forces to viscous forces. A low Reynolds number means that viscous forces are predominant over the inertial ones. The viscous dominance over the inertial forces, means that the flow falls into the laminar regime, while a high Reynolds number indicates that the inertial forces dominate which results in a turbulent regime.³⁸

The Reynolds number can be written as,

$$Re = \frac{U_0 L \rho}{\eta} \quad 7$$

where U_0 is the mean velocity, L is the hydraulic diameter of the channel, ρ is the fluid density and η is the dynamic viscosity of the fluid. The hydraulic diameter of the channel can be written as a function of the area of the cross section of the channel (A) and the wetted perimeter (P_{wet}).

$$L = \frac{4A}{P_{wet}} \quad 8$$

The resultant laminar regime, is responsible by two effects in the flow, one is that diffusion is the dominant mass transfer process, and the other is the flow velocity that depends on the boundary conditions, which results in a parabolic velocity profile where the velocity is maximum in

the centre and zero at the walls, Figure 1.13.⁴³ This parabolic flow profile is known as Poiseuille flow.



Figure 1.13: Axial velocity flow profile inside a microchannel. The velocity U_z is independent of the position along the z axis, but it is dependent of the position in the y axis thanks to the no-slip boundary conditions. This means that the maximum velocity is in the centre of the channel and decreases as its position is closer to the walls of the microchannels.

The velocity in these regimes is constant along the stream lines that roam the microchannel but, it varies across the channels width. The no-slip boundary condition forces the velocity to be zero at the walls of the microchannels and so, as we move towards the centre of the channel the velocity increases until it gets to its maximum at the centre of channel. The velocity gradient is therefore maximum close to the walls, and minimum at the centre, leading to high shear forces near the walls.

Mixing in these conditions is done by diffusion. Diffusion is mediated by the concentration gradient, i.e. molecules tend to move from a more concentrated region towards a less concentrated one by Brownian motion.

1.3.2. Péclet number

Reynolds number in microfluidic devices is usually low, generating a laminar flow regime where diffusion is the dominant mass transfer process. But diffusion alone is a long time-consuming process since it depends mainly on Brownian motion. The Péclet number, also a dimensionless number, can provide some insight on the relative importance of diffusion dynamics to convection dynamics.

The Péclet number can be written as,

$$Pe \equiv \frac{U_0 \times w_f}{D_S} \quad 9$$

where w is the channel width and D the diffusion coefficient. And so, it is dependent on channel width, flow average velocity and on the diffusion coefficient. The Péclet number increases as we

increase the width and flow average velocity, and this indicates that mass transport by convection is more significant than transport by diffusion. In opposition, a decrease in the channel width decreases the Péclet number, which will increase the relative importance of mass transfer by diffusion.

From the Péclet number, it is possible to acquired estimates on how much time it is required to achieve mixing for a given channel width. This time τ , can be estimated through:

$$T_D \sim \frac{w_f^2}{D_S} \quad 10$$

From Eq. 10, it is easy to notice that the time also increases as the width of the channel increases, since the molecules need more time to travel the larger distances. The same also happens for the channel length requirement, as the width of the channel increases, the mixing process occurs slower and so, a longer channel is required. The required distance that a molecule has to travel along the microchannel in order to achieve mixing can be estimated as

$$Z \sim \frac{U_0 \times w_f^2}{D_S} \quad 11$$

1.3.3. Mixing techniques

As seen above, mixing in microfluidic devices can be too slow to be practical. This is mainly due to mixing being mostly mediated by diffusion and to the small contact area between fluids. Fortunately, many mixing techniques on microfluidic devices have been developed to improve the mixing efficiency.

These mixing techniques can be divided into two main groups, active mixing and passive mixing techniques.

The active mixing techniques rely on energy inputs to perturb the flow dynamics, and with that increase the contact surface area between fluids enabling a faster mixing. On the other hand, passive mixers rely mainly on the device design and the flow rate ratios chosen (Q_k) to provide the same outcome.

1.3.4. Active mixing techniques

Active mixing happens whenever energy inputs are provided into the systems. These energetic inputs can be given either by the use of magnetic particles under magnetic fields, acoustic waves, electrokinetic time pulsed pressure perturbation and thermal perturbations.^{44–47}

Although active mixers have historically performed better than the passive ones, possessing shorter mixing times and shorter channels lengths, they require complex fabrication processes that often reveal to be quite expensive and difficult to integrate with other fluidic components. Also, often they have been indicated as non-compatible with biological samples thanks to the secondary effects of the energy inputs they require.⁴⁶

1.3.5. Passive mixing techniques

Passive mixers also intend to increase the contact area between fluids, but unlike their counterparts, they do not require energy inputs. They rely mainly on two subjects, the device special design and the flow conditions present (like the flow rate ratio). Moreover, they do not require complex fabrication procedures and can be easily integrated with other fluidic components.⁴⁶

The herringbone staggered device is an example of this technique,⁴⁸ so as the barrier induced device,⁴⁸ or the in the case of this work the flow focusing devices.^{49,50}

Flow focusing techniques consists on squeezing an inner fluid with an outer sheath of another fluid. Usually, the device is composed by three inlets and the middle one comprises the stream that will be squeezed by the two side solutions injected from the side inlets, Figure 1.14 - A.

The flow rate ratio (Q_R) between the sides and centre fluids can be defined as:

$$Q_R = \frac{aQ_s}{Q_c} \quad 12$$

where Q_s is the flow rate of each side stream, a is the number of side streams, and Q_c is the flow rate of the centre stream.

When predicting how the width of the centre stream varies with the Q_R in 2-D microfluidic devices, it is important to assume that the flow in the microchannels is steady and laminar, all fluids are Newtonian and have the same density in all the microchannels, and for last, all the microchannels need to have the same height.⁵¹

For squeezing the centre stream, one must consider the mass conservation principle where the total flow rate (Q_T) inserted in the microfluidic device, is the same that exits the device and so,

$$Q_T = aQ_S + Q_c \quad 13$$

This principle is also of use when predicting the focused stream width, considering that the (Q_c) inserted has to be the same of the focused stream,

$$Q_c = w_c \bar{v}_c h = Q_f \quad 14$$

where w_c is the width of the stream, \bar{v} is the average speed of the stream and h is the height of the microchannel.

From this, one can predict the width of the focused stream (w_f) as,

$$w_f = \frac{Q_c}{\bar{v}_f h} \quad 15$$

Since the average velocity of the centre stream is difficult to determine (note that the average velocity of the central stream is different from the average velocity U inside the channel), a more convenient way of estimating the width of the centre stream is through

$$w_f = w_{channel} \frac{Q_c}{Q_c + aQ_S} \quad 16$$

where $w_{channel}$ represents the width of the outlet channel.

As the side solutions squeeze the centre stream, the resulting focused stream acquires a different width. However, this width is not constant throughout the cross section of the microchannel, and thanks to the mass conservation principle mentioned above, the amount of fluid that was being injected in the centre inlet needs to be the same as the one being focused. This effect generates a stream width with a concave form, which results from the hydrodynamic focusing applied by the side solutions and by the liquid-solid interface at the upper and bottom walls of the microchannels, where the velocity is minimal.

This effect is of particular importance, since it can correct some of our judgements when trying to measure the w . Considering that to measure the w in our work, we use pictures of the bottom or top plane views of the microfluidic device, what is being measured is not the w but the

width at the bottom or top wall of the microchannel, whose widths are significantly larger than the one at the middle height of the microchannel, Figure 1.14-B.

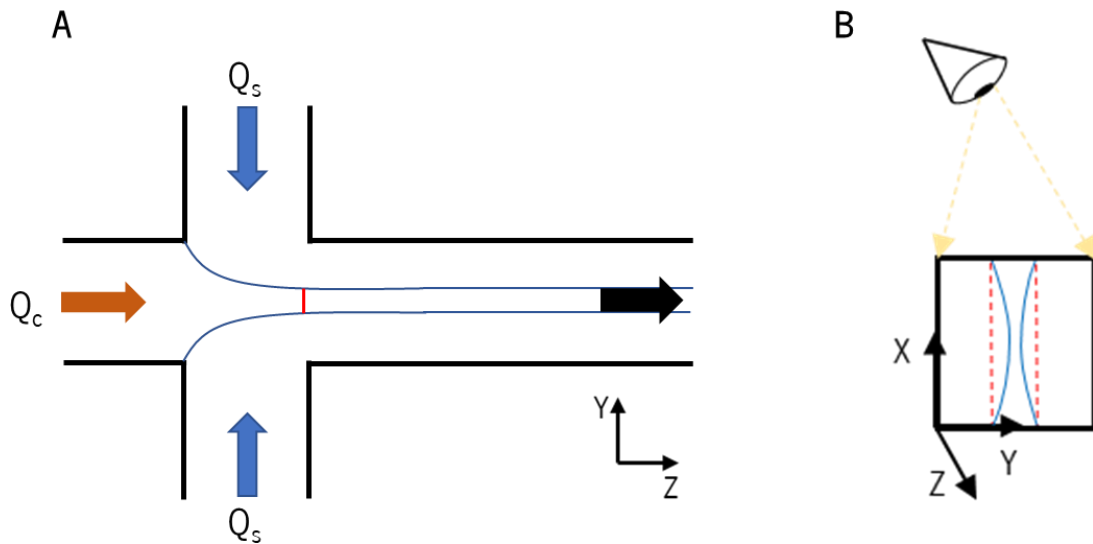


Figure 1.14: Hydrodynamic focusing effects over the fluid streams. A) is a schematic top view of how the hydrodynamic focusing is visualized using a microscope. It can be noted that, the centre stream (\rightarrow) is squeezed between two side fluids that come by the side inlets ($\uparrow\downarrow$). B) it's a schematic representation of the difference between stream width that is seen when using a microscope (grey dashed lines) and real focused stream width (blue lines). The view obtained is not of the focused width, but it is of the width of the focused stream at the microchannel walls. This width is significantly different than the focused one at the middle height of the microchannel, in the x axis.

The differences in the width of the focused stream can be attenuated by using a 3-D hydrodynamic focusing device. Usually in these devices the focused stream is not able to contact with the channels walls.⁵² Although promising, these type of devices possess a high cost of production allied with more complex procedures in the photolithography steps.

1.3.6. State of art: Microfluidic devices for particle synthesis

Microfluidics have been linked with particle synthesis for a long time.⁵³ The need to control the conditions in which oil in water or water in oil droplets were formed was one of the mains reasons for its development as particle synthesis devices. The first works on this issue showed that it was possible to obtain monodisperse sized droplets. It was also demonstrated that it was not only the dimension on the microchannels that dictated these particles size, but also flow parameters such as the Q_R could influence it.⁵⁴⁻⁵⁷

Varying the Q_r resulted in smaller or bigger droplets depending on the Q_i inserted. The trend was, an increase in the Q_r led to a decrease in the focused stream which resulted in the breakdown into smaller droplets.⁵⁴⁻⁵⁷

It did not take too long until these ideas were applied in lipid dispersions. The bulk synthesis methods for these types of nanoparticles led to considerable polydispersity. The dimensions in which the mixing was to occur, was in the centimetre length scale, and here both chemical or mechanical conditions are not homogeneous which leads to different mixing domains and results in heterogenous dispersion populations.

Jahn et al. (2004)⁴⁰ demonstrated that it was possible to form monodisperse vesicles with tuneable sizes using microfluidic hydrodynamic focusing. The concept consisted on the same used for droplets, but now using miscible solvents – that is, using a solvent shifting approach, where the lipids dissolved in isopropanol were flowed through the centre stream, and the water flowed through the side inlets. An increase in the Q_r resulted in the decrease of the focused stream which led to a decrease in the particles size. After this work, many other works tried to improve the technology and apply it for different types of formulations.⁵⁸⁻⁶¹

Microfluidic devices were used for the production of lipoplex particles. These particles consist on the use of lipid molecules associated with genetic material, like DNA or RNA. Koh et al. (2010)⁶² compared a bulk method with the microfluidic hydrodynamic focusing method and the results showed that smaller and monodisperse sizes were obtained for the lipoplexes synthesised using microfluidic devices, while at the same time not changing the inner structure and allowing a better encapsulation efficiency.

The formation of core-shell nanoparticles is of main relevance in many therapy strategies, whether for treatment or diagnosis. Valencia et al. (2010)⁶³ demonstrated that it was possible to produce particles of this type with controlled monodisperse sizes using microfluidic devices with hydrodynamic focusing.

Jahn et al. (2010)⁶⁴ when forming unilamellar lipid vesicles suggested that, the hydrodynamically focused alcohol stream width, alcohol final concentration and shear stress did not provide the main influence on the vesicle formation process. Instead, the microfluidic device geometry associated with hydrodynamic focusing mixing technique were the two main influences on the particle size dispersity, while the Q_i allowed to tune the particles size in under certain focusing regimes.

Chapter 2 - Materials and Methods

In this chapter we describe how to produce cubosomes using the solvent shifting technique in Bulk and in microfluidic devices. The procedure to fabricate polydimethylsiloxane (PDMS) microfluidic devices is also described.

The measurements and some considerations on how to obtain the central widths on the chip are demonstrated, as well as a brief description over Dynamic Light Scattering, which was the main characterization technique used.

2.1. Cubosome preparation using solvent-shifting in bulk:

The main aim of this thesis is to produce cubosomes in microfluidic devices, while manipulating the flow rate ratio to control the sizes of those particles. Because the different Q_R used imply different dilution ratios (D_R), the compositions of the initial solutions have to be adjusted. When producing the cubosomes in bulk, we used the same dilution ratios as in the microfluidic experiments for all the Q_R . In fact, in what concerns the final compositions, D_R and Q_R are exactly the same, according to:

$$D_R = \frac{V_{F127-aq}}{V_{lipid-EtOH}} = \frac{aQ_S}{Q_C} = Q_R \quad 17$$

where $V_{F127-aq}$ and $V_{lipid-EtOH}$ represent the volume of the F127 aqueous solution and lipid solution in the final sample (respectively), a represents the number of side solutions, the Q_S represent flow rate of the side solutions and Q_C the flow rate of the centre solution.

Two main compositions for the initial monoolein (Nu-check Prep Inc, Elysian, MN) solutions were used: one solution of lipid/ethanol 1/99, and another solution of lipid/ethanol/water of 1/70/29. For the different D_R (and Q_R), the initial dilution is decreased by a ratio of 10, 20, 30 and 50, and to keep the F127:MO ratio constant, the F127 concentration has to be adjusted for each D_R (and Q_R).

Cubosome were produced according to a solvent shifting approach. The procedure is done according to the work presented by Spicer et al. (2001) who used a water miscible solvent to dissolve the lipid before mixing it with water, avoiding the need to input significant amounts of energy.^{29,31}

To form the cubosomes, a 2mL Eppendorf with a specific volume of F127 solution and a stirring bar was left on top of a magnetic stirrer (VWR VMS C7) at room temperature and at 1,5 Mot. After 2 minutes, a specific amount of lipid solution is injected inside the Eppendorf and left for stirring for an additional 2 minutes before removing the Eppendorf from the magnetic stirrer, and the stirring bar from the solution, Figure 2.1. The calculated values for the F127 solutions and lipid solutions are depicted bellow in Table 2.1.

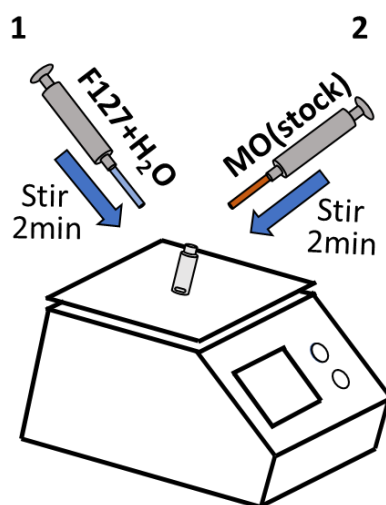


Figure 2.1: Schematic representation on how to produce cubosomes using a solvent-shifting approach in bulk. The F127 solutions are put inside a vial that contains a stirring bar and is left for stirring for about 2 minutes. After that, a lipid stock solution is fiercely injected inside the vial and left for stirring for 2 extra minutes. At the end, the vial is recovered from the magnetic stirrer and the stirring bar recovered.

Table 2.1: Volumes for mixing the lipid solutions, Monoolein with ethanol or Monoolein with ethanol:water mixture, with the F127 solutions to produce cubosomes with different batches of lipid solutions by the method described by Spicer et al.³¹ The solutions volumes are related with each Dilution factor that corresponds to a specific Flow Rate Ratio that was studied in the microfluidic devices.

Q_R	D_R	F127	MO:EtOH	MO:EtOH:H2O
		Vol. / μ l	Vol. / μ l	Vol. / μ l
10	10	909	91	91
20	20	952	48	48
30	30	968	32	32
50	50	980	20	20

2.2. Cubosome preparation using solvent shifting in a microfluidic device:

To prepare cubosomes using a microfluidic approach, two microfluidic devices were used. One made of Cyclic-Olefin-Copolymer (COC) (catalog no. 02-0757- 0166-02, Microfluidic ChipShop), and the other made of polydimethylsiloxane (PDMS).

Figure 2.2 demonstrates how the microfluidic setup was assembled. The side syringes were filled with water and F127, who worked as a stabilizer for the cubosomes. These syringes were place together on the same syringe pump (NE-1200, New Era Syringe Pumps), while the centre syringe that contained the lipid solution was placed on a separated syringe pump (NE-300, New Era Syringe Pumps) to enable the creation and manipulation of the Q_c . The outlet channel was connected to an Eppendorf using Teflon tubing (1548L, IDEX).

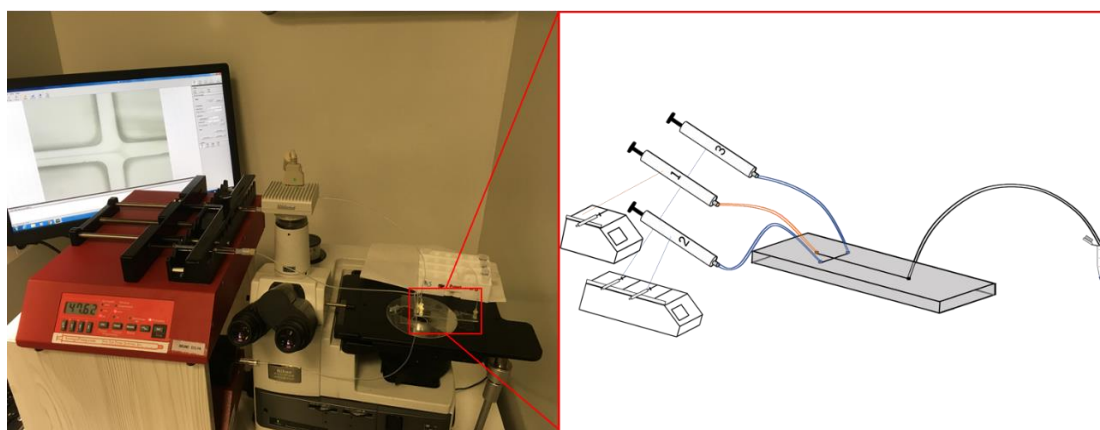


Figure 2.2: Picture of the setup made to produce cubosome particles using a microfluidic device with two syringe pumps and one microscope, to monitor the flow conditions. The inset represents a schematic view on the microfluidic device. Where the syringe 1, placed in the smallest syringe pump, contained the lipid stock solution and was connected to the centre inlet, while syringes 2 and 3 were placed together in the biggest syringe pump and contained the F127 solutions connected to the side inlets. Both three streams met at cross junction of the device, where the centre stream was hydrodynamically focused by the two side streams. After meeting at the cross junction, the three streams flowed together towards the outlet where they were collected at 4 (Eppendorf).

2.2.1. Preparation of Polydimethylsiloxane devices:

To prepare a microfluidic device we followed the procedure describe by Whitesides and McDonald (2002)⁶⁵ which relies on drawing a mask with a CAD program and then print it with a high precision printer. This mask would later be used in a photolithography process to obtain the SU-8 master for the PDMS to be poured in.

To produce the device, we started by designing the microfluidic device on AutoCAD 2007. After designing the mask, we printed it and took it to the Clean Room where a photolithography process was performed following the protocol established by MicroChem SU-8 2000, Figure 2.3–Phase I.

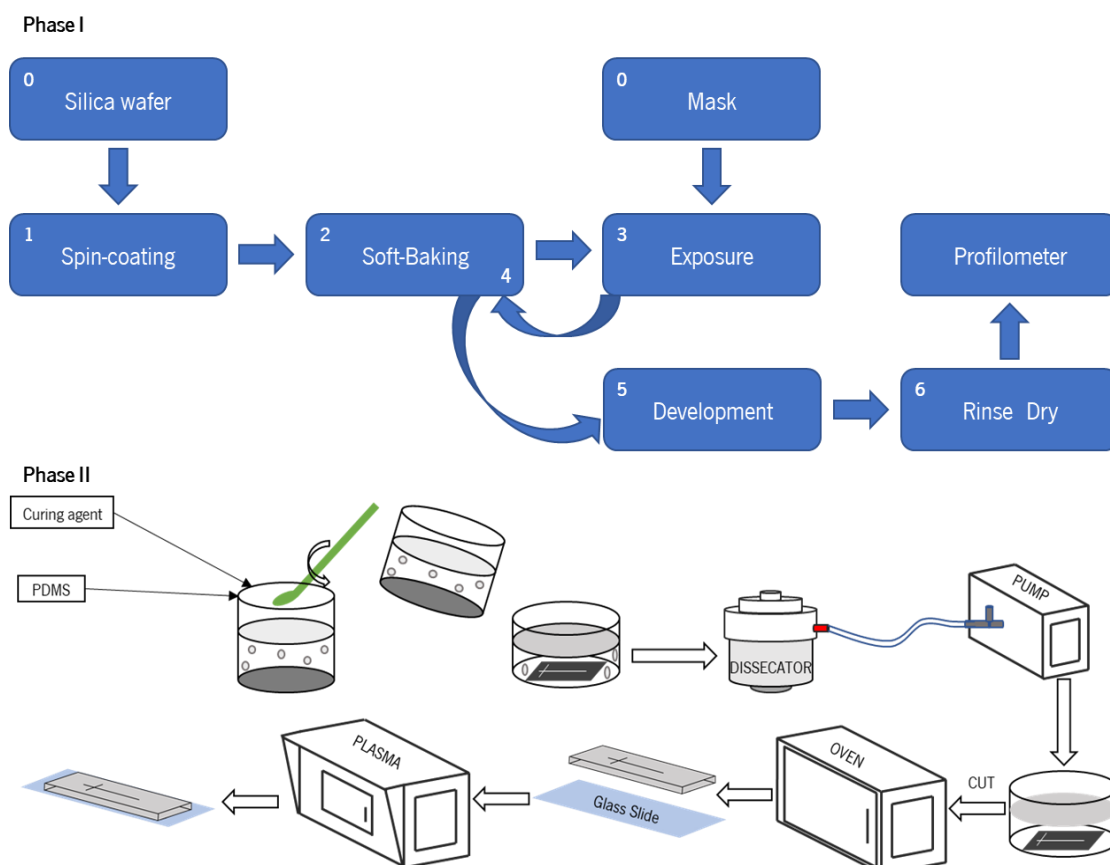


Figure 2.3: Schematic representation on, how to produce a PDMS microfluidic device. The process is divided into two phases, I and II. Phase I described the process in which the silica wafer is produced, with each number representing the order of the events, to work in phase II as a mould for the PDMS batch. The Phase II describes the process of producing the microfluidic device using the PDMS mixture with the cross linker (10:1). After mixing they are mixed with a spatula until it acquires a whitish aspect. The air bubbles are removed with the vacuum, at the dissector, and then the object is put into the oven, at 65°C for at least 2 hours to cure the PDMS. The PDMS is then peeled off from the wafer, and the inlets are made with a plunger. With a clean glass slide, and with the PDMS cleaned, both are put under plasma treatment, to allow the irreversible linkage between them.

The process is relatively simple from the moment the SU-8 wafer is made. Figure 2.3-Phase II describes how the device was obtained from the moment the PDMS was mixed with a cross linker (184 Silicone Elastomer, DOWSIL™) at a 10:1 mass ratio, respectively.

The previously mixed PDMS was poured on the SU-8 master and then it was taken to the dissector to remove the air-bubbles. After removing the bubbles, both were put in an oven at 65

°C for at least 2 hours. With this increase in temperature the PDMS was cured and became more rigid.

The PDMS chip plus master were then retrieved from the oven and the chip peeled off the SU-8 wafer by cutting the PDMS on the edges. For making the tubing entrances, a puncher was used. The sealing of the chip was done with a glass slide after cleaning both the glass and the PDMS with absolute ethanol and water. After, the cleaned PDMS chip and glass slide had their surfaces exposed to an oxygen plasma (Plasma Cleaner PDC-002-CE, HarrickPlasma) for about 25 seconds.

Finally, after exposing both to the oxygen plasma the surfaces were reactive and could be linked by just putting them into conformal contact.

2.2.2. Channel surface functionalization:

The PDMS device has its channels with a hydrophilic character after the plasma treatment, because its surface becomes oxidized, however this effect decreases relatively fast when the surface is in contact with air.⁶⁶ To make the surfaces hydrophilic in a permanent manner, the channels surface need to be treated with a coating solution otherwise it will not have a good wettability profile and nonspecific adsorption of hydrophobic analytes may occur.^{66,67}

F127 at a 0.3 wt% dissolved in Mili-Q water was used to coat the surface of the channels. This solution was used both in the PDMS device and COC device, which will be introduced later. The Pluronic F127 belongs to a group of co-polymers constituted by three blocks $(\text{PEO})_m (\text{PPO})_n (\text{PEO})_m$, which in the case of F127 m and n represent a mean value of 100 and 65, respectively. The PPO group has a hydrophobic character and is known to adsorb onto hydrophobic surfaces by hydrophobic interactions whilst the PEO groups have a hydrophilic character and stay turned into the aqueous medium.^{66,68}

To coat the channels of the devices the solution was flown in all the inlets and left inside the device for at least two minutes before starting any experiment.

2.2.3. Particle preparation using Solvent Shifting in a microfluidic device:

To use the microfluidic device, two glass syringes of 500 μl (750LT SYR, Hamilton) were used to inject the F127 solutions and one glass syringe of 25 μl (702N SYR, Hamilton) was used

to flow the lipid stock solutions, unless mention otherwise. The final mixed solution was collected at the end of the outlet channel with an Eppendorf.

To connect the syringes to the microfluidic device, we used always Teflon tubing (1548L, IDEX). To connect the syringes to the tubing, blunt needles that connect to the syringe via a Female/Male Luer connection, and to the tubing through the needle, were used. On the other hand, in the case of COC devices, which have Female Luer connectors, we glued a Male Luer connector to the tubing, fixing it with epoxy (instant 90s, Araldite®). This assembly connected directly in the device. The connectors used for the PDMS device were different, with this type of device there was no need to use a connector between the tubing and the device because the tube was plunged directly into the entrances.

After filling the syringes and connecting them to the device, the syringes were put in different syringe pumps (NE-1200 and NE-300, New Era Pump Systems), previously programmed with the diameter of the syringes and the flow rate (Q) required, to allow the customization of the solutions injection. The Q_s and Q_c for each syringe is shown below on Table 2.2 and was calculated using Eq. 13.

Table 2.2: Flow rates used in each syringe pump to inject the solutions from the syringes to the microfluidic device for each of the Q_k used, at two different Q . The values for the Q sides are representative of the flow rates of the syringes that contain F127 solution and Q centre for the syringes that contain the lipid solutions.

Q_k	$Q = 20 \mu\text{l/min}$		$Q = 100 \mu\text{l/min}$	
	Q sides $\mu\text{l/min}$	Q centre $\mu\text{l/min}$	Q sides $\mu\text{l/min}$	Q centre $\mu\text{l/min}$
10	18.182	1.818	45.455	9.091
20	19.048	0.952	47.619	4.762
30	19.355	0.645	48.387	3.226
50	19.608	0.392	49.020	1.961

The lipid stock solutions worked as centre solutions in the microfluidic device, Figure 2.4. The side solutions were of F127 dissolved in water, these solutions were responsible for hydrodynamically focusing the centre solution. This co-polymer composed by one hydrophobic group intercalated in the middle of two hydrophilic groups is described in literature as one of the most widely used stabilizers to prevent the aggregation of lipid dispersions.^{12,23}

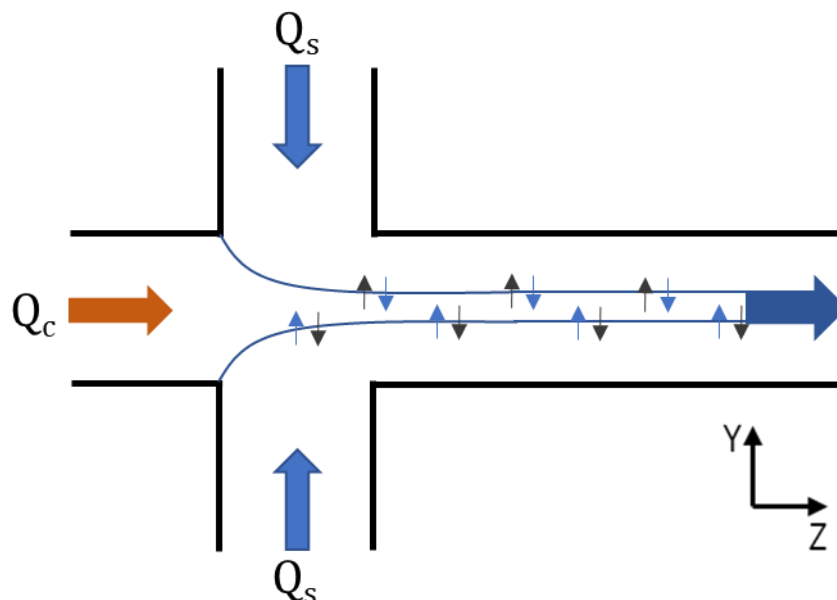


Figure 2.4: Schematic representation of the microfluidic hydrodynamic focusing approach used for controlled mixing and assembly of cubosomes of controlled size. In both setups (PDMS and COC) the microchannel width and height are ca. 100 μm . At such small cross-sections the flow tends to be laminar and mixing occurs by diffusion. By decreasing the width of the centred (focused) stream the distance that solvent molecules have to travel until mixing is achieved becomes smaller, leading to faster mixing times. The lipid stock solutions were injected in the centre inlet with flow rate Q_c , and the F127 solutions were injected in the side inlets, with flow rate Q_s . The solutions meet in the cross junction where the mixing process starts, with ethanol ($\uparrow\downarrow$) and water ($\uparrow\downarrow$) being mixed by diffusion while flowing towards the outlet, where the fluid was collected. Whereas ethanol is a good solvent for the lipids, water is not, favouring the formation of self-assembled structures. The rapid and controlled mixing of ethanol with water leads to the formation of cubosomes, whose size is controlled by manipulation of the speed of mixing.

It is important to note, that this procedure was done carefully, otherwise air would be trapped inside the system which could negatively affect the hydrodynamic focusing performance.

2.2.4. Measurements of the focused stream:

To determine the mixing time and the required channel length to achieve mixing, we measured the μ for all of the D_k studied.

To do so, we used a Nikon camera coupled in an inverted microscope (Inverted Metallurgical Microscope Eclipse MA200 from Nikon) to photograph the hydrodynamic focusing

region during the particles formation. Since ethanol refractive index is ca. 1.36 whereas the water is 1.33 the contrast between both was perceptible.

When taking pictures of the microfluidic device during the hydrodynamic focusing, it is important to note that the hydrodynamic focusing on a two-dimensional microfluidic device happens in the horizontal plane. The stream distribution at the upper and bottom walls of the device is not affected in the same intensity as it is in a middle plane, because the flow velocity is slower on the edges. This results in a concave cross-section of the flow profile, and for that reason the estimated values and measured values will differ, Figure 2.5. Although trying to be always at the upper, or bottom wall of the microchannel, the exact position could not be guaranteed to be same in all the experiments.⁶⁹

And so, when measuring w one must consider that the measurement obtained is close to the maximum values of the w .

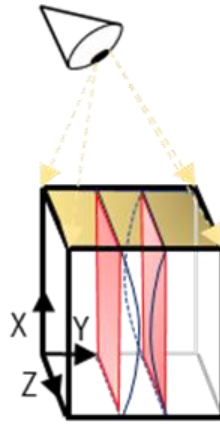


Figure 2.5: Schematic representation of the cross section of an hydrodynamically focused stream, highlighting the concave flow profile (blue lines). The microscope observation takes as a reference the top wall of the device, and therefore, the measured width (in red) of the focused stream corresponds to its maximum width, giving an overestimation of the average width of the focused stream.

With the pictures taken, it was possible to estimate the width of the centre stream and compare it with the one estimated from Eq. 16, see Table 2.3.

Table 2.3: Calculated parameters for the estimated and measured focused width (w). The Eq. 9, 10 and 11 were used to calculate Pe , τ and Z the for all the Q_k at a Q of 100 $\mu\text{l}/\text{min}$. The measured focused centre stream width is used as an indication of the difference between what is measured in the microscope, and what is calculated using Eq. 16. This difference is explained in the in Figure 2.5.

Q_k	Channel Width/ μm	$w_r/\mu\text{m}$		τ/s	Z / cm	Pe
		Estimated	Measured		$Q_t=100$ $\mu\text{l}/\text{min}$	$Q_t=100$ $\mu\text{l}/\text{min}$
10	100	9.091	20.556	0.098	1.640	1803.752
20		4.762	18.750	0.027	0.450	944.822
30		3.226	15.000	0.012	0.206	640.041
50		1.961	8.380	0.005	0.076	389.045

2.3. Characterization technique:

In this caption we describe the technique used for characterizing the particles that were obtained. Dynamic Light Scattering (DLS) was the standard choice thanks to its quickness and reproducible results while not demanding significant amounts of sample volume and allowing its recover at the end of the measurement.⁷⁰

DLS lays on two phenomena: the Tyndall Effect and the Brownian motion. As the laser from the instrument strikes a colloidal solution, the particles laying there work as mobile secondary wave sources, this movement is responsible for the occurrence of a light intensity pattern.

With the particles in a constant motion the distance travelled by the electromagnetic waves varies with time. This time dependence can be associated with the diffusion of the particles in the medium. As particles with larger hydrodynamic radius diffuse slower, the differences in intensity vary more slowly in time, and the opposite is expected for smaller particles whose motions are described as being significantly faster when compared to the previous ones, Figure 2.6-A.⁷¹

After obtained the values of the time-dependent light scattering intensity, an autocorrelation function ($g^2(T)$) can be constructed as a function of delay time T :

$$g^{(2)}(T) = \frac{\langle I(t) \times I(t+T) \rangle}{\langle I(t) \rangle^2} \quad 18$$

Where $I(t)$ is the intensity of the scattered light at a time (t) and $I(t+T)$ the light scattered at time ($t+T$), respectively.^{71,72}

The autocorrelation function is also directly related with the first order field correlation function, the field-field correlation function ($g^{(1)}(T)$) as,

$$[g^{(1)}(T)]^2 = g^{(2)}(T) - 1 \quad 19$$

When considering a solution of spherical monodisperse samples, the field correlation function can be estimated as,

$$g^{(1)}(\tau) = A \cdot e^{-Dq^2\tau} + B \quad 20$$

Describing a mono exponential decay where (A) is the amplitude of the correlation factor, (D) the translational diffusion coefficient, (q) the magnitude of the scattering vector and (B) the baseline.

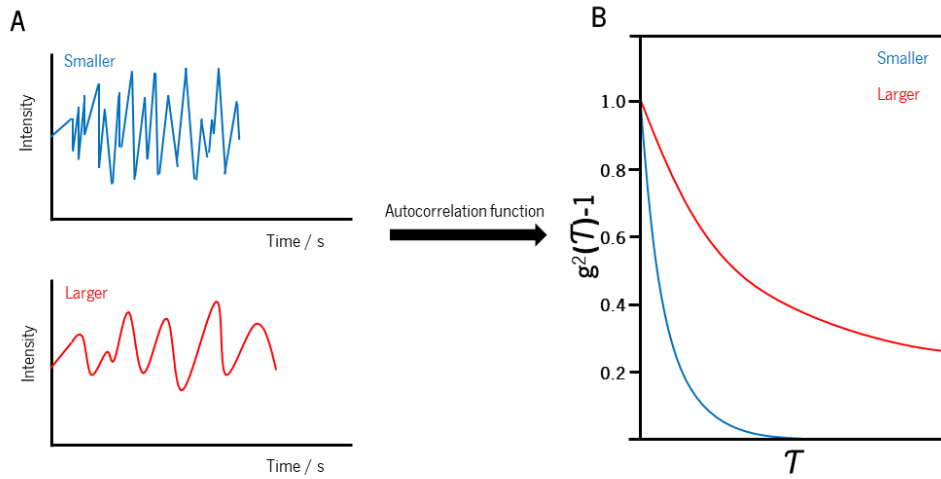


Figure 2.6: Graphical representation of a DLS measurement for larger particles (red) and smaller particles (blue). A) Light intensity profiles over time of smaller particles (top/blue) and smaller particles (bottom/red); B) autocorrelation function deduced from larger and smaller particles through different delay times. Redrawn from Hassan et al.⁷¹

With particles possessing a spherical format, the hydrodynamic radius (R_h) can be obtained from the translation diffusion coefficient (D) using the Stokes-Einstein relation,

$$D = \frac{k_B T}{6\pi\eta R_h} \quad 21$$

with (k_B) as the Boltzmann's constant, the (T) as the absolute temperature and (η) as the solvent viscosity.

When considering polydisperse samples, the monoexponential model described above is not suitable any longer since now there is a distribution of diffusion coefficients. In a polydisperse sample eq. 20 can be rewritten into a sum of exponentials, weighted by their amplitudes:

$$g^{(1)}(\tau) = \int_0^{\infty} G(\Gamma) \exp(-\Gamma\tau) d\Gamma \quad 22$$

where the decay constant Γ is defined as $\Gamma=Dq^2$, where (q) is the scattering vector.

To obtain the exponential decay rates ($G(\Gamma)$) an inverse Laplace transform can be applied to the measured correlation function but, the existence of a baseline, dust interference, measurement noise and the exponential function under the integral make this equation ill-conditioned.⁷¹

A suitable way of extracting information from moderately polydisperse samples is through the Cumulants method, which is assumed as the simplest and most reliable one.^{70,71} The Cumulants method approach lays on the calculation of the mean and variance of the distribution without considering higher moments. It is applicable only for narrow monomodal distributions.

The $\exp(-\Gamma T)$ term in equation 22 can be expanded to a mean value of $\bar{\Gamma}$ which when applied to equation 8 it stays,

$$g^1(\tau) = e^{(-\bar{\Gamma}\tau)} \cdot \left[1 + \frac{\mu_2 \tau^2}{2} \right] \quad 23$$

In our experiments, the equipment used was the Dynamic Light Scattering System SZ-100Z, where the samples were analysed at two different angles, 173° and 90° for four runs of ninety seconds each. For the dispersion medium, water diffusion and the lipid diffusion were selected for the software calculations.

Once acquired the data, a MATLAB routine was used to calculate the size and polydispersity index of the samples.

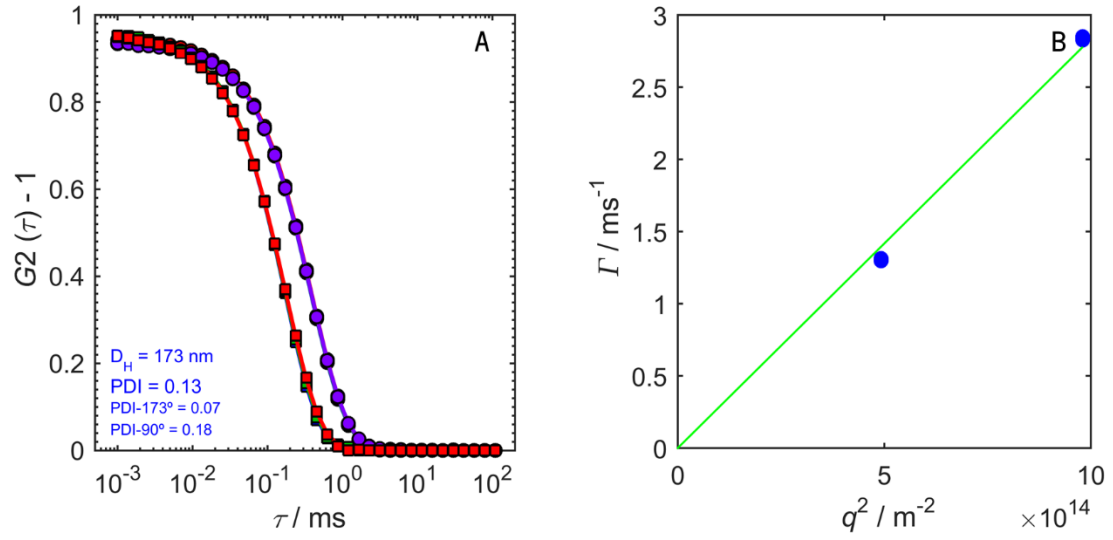


Figure 2.7: DLS autocorrelation function ($G_2(\tau)-1$) data and fitting of a representative cubosome sample. A) The sample used was produced from a lipid stock solution of monoolein:ethanol (1/99) in a COC microfluidic device at a $Q_i=100 \mu\text{l}/\text{min}$ and $Q_r=10$. The measurements were performed at two different scattering angles (90° - circles, 173° - squares), and the data fitted with the cumulants method in a home-made Matlab routine, providing the characteristic decay constant Γ and polydispersity index (PDI). B) Fitting of the obtained Γ in A as a function of the scattering vector q^2 .

Chapter 3 - Results

The results of this thesis are divided in two parts, one is related with the optimization process of the PDMS device (3.1), where a few considerations are taken into account on the microfluidic device and its compatibilities. The other one is a concrete study on the particles formation (3.2).

The section 3.2 describes the cubosome formation on bulk or using a microfluidic device (COC or PDMS), where it is also demonstrated the effect of the lipid stock solution composition, the addition of water, the increase in the lipid concentration and the use of a lipid mixture. The concentration of the stabilizer stock solution it was also a subject of study.

3.1. Formation of particles when co-flowing ethanol and water on a microfluidic device

At the beginning of our experiments we were faced with an issue regarding the PDMS microfluidic device. The use of ethanol and water (when flowing separately inside the device microchannels) promoted the formation of non-expected structures on the channels walls, whose nature is unclear. This was a relevant issue because ethanol and water were planned to be the solvents used in the solvent shifting approach to prepare cubosomes. Clearly the emergence of such objects was not compatible with our cubosome synthesis since it could interfere with their formation, make the characterization more difficult, and also interfere with the subsequent intended application of cubosomes in in-vitro studies. This led us to many troubleshooting sessions within the group throughout the initial months of the project in an attempt to understand the origin of such structures, and how to avoid their formation.

The PDMS microfluidic device was produced at our facilities. First the SU-8 master was fabricated in the clean room by photolithography, as the one described in Section 2.2.1. The microchannel width and height was 100 μm . After the master completion, PDMS was prepared by mixing the PDMS and the curing agent in a 10:1 ratio, respectively. The mixture was vigorously shaken and mixed and degassed to remove air droplets. The mixture was then poured on top of the master and degassed again to remove any air bubble formed meanwhile. After degassing, the mixture was transferred to an oven at 65°C for 2 hours leading to the PDMS cure and hardening. The PDMS device was then peeled from the master and had inlet holes punched to fit the tubing.

Subsequently the chip and a glass slide were washed and subsequently exposed to an oxygen plasma. The two plasma-exposed surfaces of the chip and glass slide were then brought into contact to complete the bonding and sealing of the device.

The three inlets worked as entry points for each of the solutions, in the centre inlet was injected absolute ethanol, and in the side inlets water. The three inlet channels met in the cross junction of the device, where the hydrodynamic focusing happened. After meeting at the cross junction, the three components were flowed towards the outlet channel, Figure 2.4.

Unexpectedly we started noticing that at the junction between the ethanol and water channels, as well as along the ethanol-water interface, small structures started to form. Since ethanol and water are miscible and presumed to be compatible with PDMS, this observation was unexpected, and not straightforward to understand. The structures at a first stage formed as small units but then after a few more minutes they continued growing –Figure 3.1.

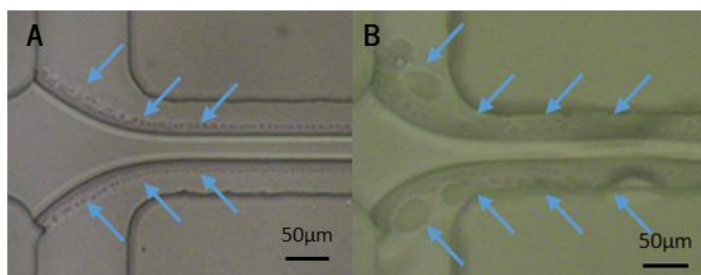


Figure 3.1: Optical Microscope images at the cross junction of the PDMS microfluidic device while injecting the solutions. Absolute ethanol was injected in the centre inlet and hydrodynamically focused at the cross junction by two side streams of water. In A) the hydrodynamically focusing enabled the formation of unexpected structures on the water sides, 1 minute after starting the experiment. B) shows the formation and deposition of these unexpected structures as they grew 34 minutes after starting the experiment. The (→) are indications of the presence of unexpected structures

It is important to note that the objects only showed in the water region, this could be an indication of the polarity of what was forming them. The formation in the water clearly demonstrated that these structures were of hydrophobic nature. Another indication of this statement is reflected when we tried to clean the channels after the experiments. The objects could only be washed out with ethanol and not water.

These two points made us realize that the ethanol could be the carrier for the components forming these structures, as if they were dissolved in ethanol and after changing to water (a presumably bad solvent in this situation) they just aggregated and precipitated – just like a solvent-shifting experiment would work. Still the question resided on what could be the provider of this

component. The formation of these objects was not expected, since all the materials are classified as having a good compatibility for ethanol.

The group formulated three hypotheses on what could be the reasons, and they are as follows:

- i. The occurrence of the objects was a result of an impurity in our solvents (ethanol or water), and here we also tried the use of 2-Propanol (IPA) instead of ethanol, as well as different grades of ethanol, and water from different sources;
- ii. The materials used in the setup (e.g. chip, connectors, tubing, etc) were not 100% compatible with absolute ethanol, even if the chemical charts said the opposite;
- iii. The objects formed could be the result of more than one factor at once, like the tubes and the PDMS device.

These hypotheses allowed us to start removing possible factors in our experimental design.

At first, we tried to see if there was any impurity in the experimental components. We used different batches of PDMS and cross-linker to produce new microfluidic devices, and different batches and grades of ethanol, IPA and water, still they did not inhibit the objects formation. And so, the materials compatibility had to be considered.

An examination of the chemical-compatibility charts indicated that the materials used possess a good compatibility with the solvents tested. However, we hypothesize that one of the components could have some impurity that was being dissolved as the ethanol passed through and precipitated when mixing with water at the junction.

In order to see the possible sources for the objects formed, the materials were changed one after another to track any kind of advance. The materials tested were as follows:

- Different syringes, glass ones from Hamilton Gastight with a Teflon tip in the plunger (750LT SYR, Hamilton), and Plastic syringes (Terumo® Syringe Without Needle, Terumo®) made of polypropylene with a rubber tip in the plunger;
- As for the connections between the syringes, female-male Luer connectors made of PEEK (Polyetheretherketone) and ETFE (Poly(Ethylene Tetrafluoroethylene)) (Luer Adapters, IDEX), as well as Luer plastic-metal needle tips (Agani Needle 24G, Terumo®) were used;
- Two different types of tubes were used, EVA (Ethylene Vinyl Acetate) (Cole-Parmer) and Teflon (politetrafluoretileno) (1548L, IDEX);
- We also considered that the silicon wafer could be providing some kind of material, and so we produced more than wafer, with and without priming the silicon/SU-8 with silanes;

- The solvents, as mentioned before were also changed, more than one batch and grade of ethanol (99.8%, Sigma-Aldrich; Ethanol for gas chromatography, SupraSolv[®]), IPA (99.8%, Honeywell) and Mili-Q water were used.

After testing the above mentioned materials, the objects were still forming in all the experiments, even though the materials were described as possessing good compatibilities. The only option left was the PDMS device itself.

Indeed, when changing from the PDMS device to a COC device, the objects did not appear any longer. To the best of our knowledge, this was never reported before and PDMS is regarded as chemically compatible with ethanol. The only remark about the use of PDMS with ethanol is that PDMS swells slightly, but such behavior is reversible.²² We hypothesize that either some non-crosslinked PDMS or unreacted cross-linker are being solubilized by ethanol, and when mixing with water occurs, precipitation of the solubilized chemical takes place.

One option was then to simply discard the use of PDMS, however PDMS provides a unique advantage over other materials, which is the ability to design and make our own devices with a design optimized for a particular application. As such, we decided to investigate the possibility of using PDMS devices for solvent-shifting without the problem of impurities showing up.

The idea that the PDMS device was affected by the use of either ethanol, or IPA, forced the group to look for two options, change the organic solvent used or somehow diminish its effect of ethanol on the PDMS device. The idea of changing the solvent was clearly the less interesting, since it would require to change some of the plans for the upcoming experiments. As such, we decided to investigate the effect of decreasing ethanol strength.

To diminish the ethanol strength, it was decided to mix the absolute ethanol in water until the objects were no more seen inside the microfluidic device, Figure 3.2. This dilution would be made before injecting the mixture inside the device. To inject the ethanol/water mixture, the most compatible materials were chosen, i.e. glass syringes, Teflon tubes and female-male luer connectors made of PEEK and ETFE.

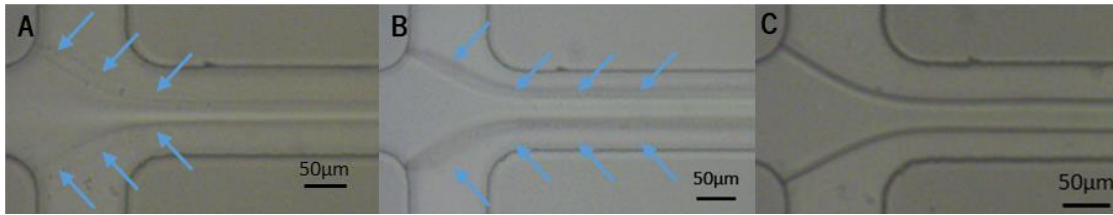


Figure 3.2: Optical microscope photograph from the cross junction of a microfluidic device, where absolute is squeezed by two water side streams. A) The ethanol stream is composed by ethanol at 82 wt% dissolved in water. B) The ethanol stream is composed by ethanol at 78 wt% dissolved in water. C) The ethanol stream is composed by ethanol at 76 wt% dissolved in water. The (→) are indicatives of the objects presence.

As we decreased the ethanol content in the centre stream, we kept having objects formed until we reached an ethanol composition of 76 wt%. At this no more objects were visible in the microfluidic device, Figure 3.2–C, but a prolonged flow time (~5 hours) did start to show some objects again. We repeated the experiment with a new device and we stopped seeing the objects. This finding somehow showed us that the PDMS devices have some kind of life time until they start forming the objects again, Figure 3.3.

By reducing the ethanol amount to 70 wt% we did not spot the formation of objects even after wait times close to 8h of continuous flow. These were the conditions we used when making cubosomes.

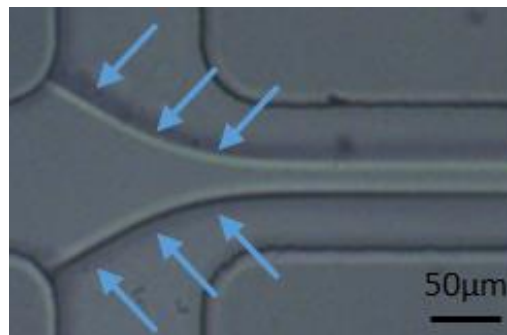


Figure 3.3: Optical microscope image at the cross junction of a PDMS microfluidic device while flowing ethanol at 76 wt% dissolved in water as the centre stream and water as the side streams. This device had at least five hours of continuous usage, and after this how structures we starting to form and precipitate at the microchannel walls, represented by the (→).

3.2. Cubosome production using the solvent shifting technique

The solvent shifting approach involves the solubilisation of the lipid in a solvent that is miscible with water in a first step. In a second step, this solvent-lipid mixture is injected in an aqueous solution, with the mixing of the two solvents inducing the formation of self-assembled structures. Spicer et al. determined that the solubilisation of monoolein in ethanol and subsequent mixing with a water solution containing the stabilizer F127 was a viable way to produce cubosomes, and furthermore determined the partial ternary monoolein-ethanol-water phase diagram.³¹ In the present work we explored the formation of cubosomes when departing from two types of initial solutions. In one case, monoolein is dissolved in pure ethanol, whereas in the other, monoolein is dissolved in a mixture of absolute ethanol and water. The addition of water to the initial solution was performed in a region of the phase diagram where the system is in a single solution phase. Since cubosome formation results from the mixing of ethanol with water, it was anticipated that including some water in the initial solution could be an additional way of manipulating the particle formation kinetics, and thus the size. A second motivation to study some pre-mixing of water was related with reducing the ethanol amount on the final solution, making it easier to remove when utilizing these particles in biological studies. Finally, as a third motivation, we have noticed that flowing pure ethanol in PDMS devices led to the emergence of unexpected particles at the mixing point of ethanol with water, see 3.1. Although further studies are necessary, we hypothesize that pure ethanol may dissolve some component within the PDMS microfluidic device and precipitate it again when mixing with water. This phenomenon was not spotted when flowing mixtures of ethanol/water 70/30, nor when using COC devices at any ethanol concentration.

Besides the information provided in the phase diagram, we determined the maximum water amount that could be added to an initial 5 wt% monoolein solution in ethanol. The test consisted in the stepwise addition of water until macroscopic phase separation was detected.

This occurred at a final composition of ca. monoolein/ethanol/water of 4.8/67.5/27.7 wt% which should be within the isotropic solution phase in the reported phase diagram, but in our case, was the onset of phase separation. After detecting this limit for water use, one of the most used initial solutions had a composition of 1/70/29 and showed no phase separation by visual observations, nor any noticeable aggregate under the optical microscope.

3.2.1. Cubosome preparation: solvent shifting on bulk vs solvent shifting in microfluidics

i. Solvent shifting in Bulk

In Figure 3.4 the sizes of particles formed by solvent shifting in bulk as a function of the D_k are shown. In this solvent shifting method, D_k is simply the ratio of the volume of aqueous solvent added ($V_{F127-aq}$) to the volume of the initial lipid-ethanol solution ($V_{lipid-EtOH}$).

In these experiments, the ratio between stabilizer and lipid is kept constant at 1:1. The compositions of the initial and final solutions as well as the average particle sizes, standard deviation and average polydispersity index (PDI) can be found in Table 3.1. As can be seen in Figure 3.4, the average size of the particles does not show a strong dependency with D_k except for $D_k=50$, where a noticeable (and unexpected) increase is observed. This trend is similar regardless of using a lipid stock solution with or without water, but on average the samples containing water in the initial solution showed slightly smaller sizes than samples without water. As for the standard deviation of the average sizes, there were no large deviations detected for most of the cases. The PDI obtained from these samples indicated that all of them are relatively monodisperse, which is a good indication since this method is also known for creating vesicles when forming the desired particles.³⁰

Table 3.1: Solvent shifting in bulk results summary. The initial and final compositions of F127 aqueous solution and final lipid concentration were adjusted to span a D_k from 10 to 50 while keeping a constant lipid:F127 mass ratio of 1. The corresponding average sizes, standard deviations and PDI of the particles obtained when using initial solutions containing only lipid-ethanol and solutions containing lipid-ethanol-water are also shown.

D_k	F127 wt%		MO wt% final	MO/C ₂ H ₆ O			MO/C ₂ H ₆ O/H ₂ O		
	initial	final		D_H / nm	Std. Dev. / nm	PDI	D_H / nm	Std. Dev. / nm	PDI
10	0.100	0.091	0.091	122	1	0.14	111	2	0.12
20	0.050	0.048	0.048	132	2	0.14	112	8	0.12
30	0.033	0.032	0.032	130	3	0.12	120	1	0.13
50	0.020	0.020	0.020	172	9	0.21	154	5	0.19

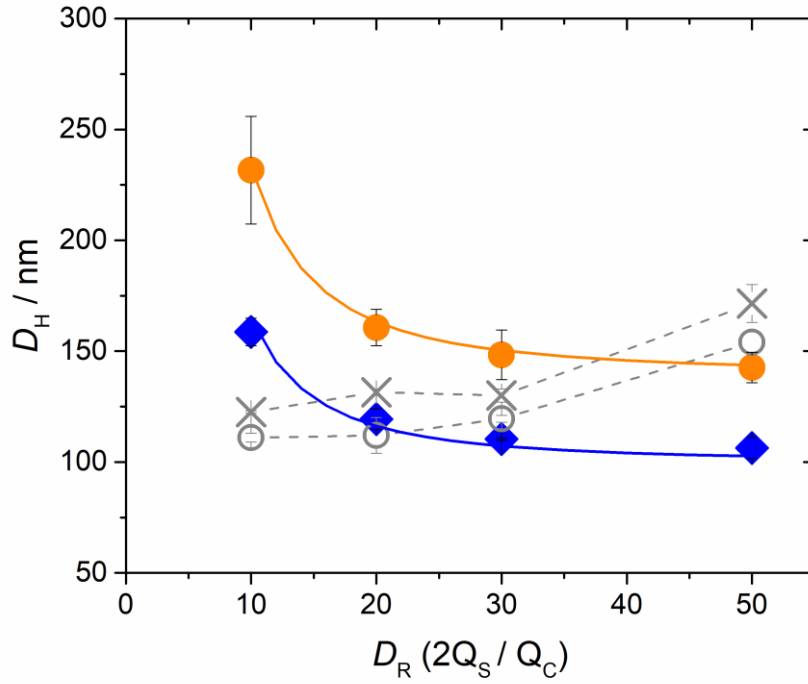


Figure 3.4: Average hydrodynamic diameter of particles formed by solvent shifting in bulk and using a COC microfluidic device. The dilution ratio (D_R) used for the preparation of the particles in bulk is equivalent to the flow rate ratio (Q_R) used to prepare the particles in the microfluidic device. Both (X) and (○) represent the average sizes for cubosomes prepared with solvent shifting in bulk. Where (X) is for cubosomes formed with a lipid stock solution of monoolein in absolute ethanol (1/99), and (○) represent the ones formed with a lipid stock solution of monoolein dissolved in an absolute ethanol:water mixture (1/70/29). The filled symbols (●) and (◆) represent the sizes of cubosome particles formed in the microfluidic chip, with (●) corresponding to particles obtained from a lipid:ethanol (1/99), and (◆) to particles obtained from a lipid:ethanol:water (1/70/29) stock solutions. Each data point corresponds to the average of at least two independently prepared samples. The solid lines represent fittings to the equation $D_H = A (D_R + 1)^2 + B$ (Eq. 28) with the fitting parameters A and B being 9300 and 140 for monoolein:ethanol, and 6500 and 100 for the monoolein:ethanol:water initial solutions, respectively. The dashed lines are guides to the eye. The excellent fit suggests the suitability of the model relating the cubosome size with the speed of mixing, controllable by D_R .

The mostly flat dependence of the particle size as a function of D_R (except for $D_R = 50$) indicates narrow possibilities to control particle sizes using normal bulk methods. Yet, the reproducible observation of larger particle sizes when $D_R = 50$, although without easy explanation, together with the observation of smaller sizes obtained when pre-mixing the lipid-ethanol solutions with ethanol does provide some prospects of using bulk methods to tune the cubosome sizes within some relatively narrow range. The relatively small polydispersities and small standard deviations are also good indications. The fact that pre-mixing water leads to smaller particle sizes could be related with the solvent shifting proceeding faster, which leads to the lipid molecules becoming amphiphilic in the solvent mixture at earlier times and resulting in a faster nucleation and growth

process that results in smaller particles. As will be seen below, this effect is also observed in the microfluidic devices.

ii. Cubosome preparation by solvent shifting using a COC microfluidic device

In this section we introduce the use of microfluidics with hydrodynamic focusing with the goal of further controlling the size of the cubosome particles formed, in analogy with the pioneering work of Jahn et al. who demonstrated that liposome size could be controlled using microfluidics.⁴⁰ In this dataset the total flow rate (Q_t) is fixed to 100 $\mu\text{L}/\text{min}$, while the flow rate ratio (equivalent to dilution ratio as discussed above) is varied from $Q_r=10$ to $Q_r=50$. The device is a two-dimensional microfluidic chip made of Cyclo-Olefin-Copolymer (COC) from microfluidic ChipShop. The device had its channels with 100 μm width and height, and a channel length of 8.2 cm, Figure 2.4. As in the bulk preparation of cubosomes, in order to keep the F127 to lipid mass ratio constant, the initial composition of F127 aqueous solutions has to be adjusted for each Q_r . Table 3.3 shows the concentrations used for the F127 solutions at each of the Q_r in order to maintain a constant mass ratio at the cross junction of 1, along with the average sizes, size standard deviation, and PDI of the particles prepared with the microfluidic device. Figure 3.4 shows the dependence of the average sizes of the particles obtained for the different Q_r (or D_r). As can be seen, in comparison with the particles formed in bulk, in this case there is a clear decrease of the particle size when D_r is increased as also found for liposome systems in the work of Jahn et al.⁴⁰ The decrease in size is more abrupt in the beginning for smaller D_r , and less pronounced for larger D_r . This is the case for both types of initial solutions (with and without an initial concentration of water), and as in the bulk case, also here particles prepared from initial solutions containing water systematically show smaller particle sizes. However, in this case, additionally, particles prepared from initial solutions containing water also show smaller standard deviations and smaller PDIs, Table 3.2.

Table 3.2: Solvent shifting results for the COC microfluidic device with constant final lipid:F127 mass ratio of 1. The particles obtained were from different lipid batches, one of monoolein 1 wt% dissolved in absolute ethanol and the other of monoolein dissolved in an absolute ethanol:water mixture (1/70/29). The average size and associated standard deviation, as well as PDI were always smaller for particles where the lipid stock solution contained water.

Q_R	F127 wt%		MO wt% final	MO/C ₂ H ₆ O			MO/C ₂ H ₆ O/H ₂ O		
	initial	final		D_H / nm	Std. Dev. / nm	PDI	D_H / nm	Std. Dev. / nm	PDI
10	0.100	0.091	0.091	232	24	0.22	159	6	0.15
20	0.050	0.048	0.048	161	8	0.17	119	5	0.13
30	0.033	0.032	0.032	148	11	0.16	110	4	0.13
50	0.020	0.020	0.020	143	7	0.16	106	5	0.13

The decrease in particle size as the D_R is increased resembles the dependency of the focused stream width (w) with increasing D_R (Figure 3.5-Figure 3.6). At larger D_R (hence Q_R) the larger flow rate of the side streams increasingly narrows the focused stream width. If the viscosities of the two fluids are similar, a rough estimation based on geometric arguments can be established for the width of the centred focused stream, through the relation:

$$w_f = \frac{w_{channel}}{D_R + 1} \quad 24$$

where $w_{channel}$ is the width of the microfluidic channel (100 μm). Figure 3.6 shows the estimated w for the different Q_R used in this work, along with experimentally determined w for initial solutions with and without water. The estimated and experimental values do not match for a variety of reasons. In first place, the assumption that the viscosities of the two solutions is the same is just an approximation. In second place, the velocity profile inside the channel is faster in the centre than near the walls, which results in a concave shape of the flow profile (Figure 3.5) with the top and bottom of the focused stream being thicker than in the centre.^{38,49} Thus, when experimentally determining w , for consistency the focus plane is always in the top wall, which results in an overestimation of w . w represents the distance over which solvent molecules have to cross in order to achieve the shift in solvent character and induce assembly of the lipid molecules. (Note that the lipid can also diffuse, but since the lipid molecules are larger than the solvent molecules, they take longer to diffuse away). Under laminar flow conditions, this molecular exchange occurs mostly through diffusion, and a rough estimate for a characteristic mixing time τ can be obtained through:³⁸

$$\tau \propto \frac{w_f^2}{D_S} \quad 25$$

where D_s is the diffusion coefficient of the solvent molecules. Figure 3.6 also shows the estimated τ , and corresponding channel length needed to achieve complete mixing (Z).

To try to gain further insight into the formation of the cubosomes, we hypothesize that cubosome size is proportional to the mixing time τ :

$$D_H \propto \tau \quad 26$$

since a slower mixing time τ would allow particles to nucleate slower and grow into bigger objects. Combining equations 24 and 25 results in:

$$\tau \propto \frac{w_{channel}^2}{(D_R + 1)^2 D_S} \quad 27$$

and consequently, combining equations 26 and 27 results in:

$$D_H \propto \frac{w_{channel}^2}{(D_R + 1)^2 D_S} \quad 28$$

Since the diffusion coefficients (D_s) of all substances remain constant across all experiments in this work, as well as $w_{channel}$ remains unchanged, one can replace these terms along with the proportionality relation by a constant A , resulting in

$$D_H = \frac{A}{(D_R + 1)^2} + B \quad 29$$

where the constant B was also added as a baseline. Equation 29 suggests that the size of the particles is inversely proportional to the square of the dilution or flow rate ratio, and provides a way to attempt fitting the experimental results using A and B as fitting parameters and test the initial hypothesis as stated through Eq. 29. A slight rearrangement of these equations also provides the following relation:

$$D_H \propto w_f^2 \quad 30$$

which directly relates the size of the particles formed with the width of the centre stream w , i.e. the narrower the focused stream width, the faster is the mixing and smaller are the particles.

As can be seen in Figure 3.4, the solid lines, which correspond to fittings using Eq. 14, manage to fit the data extremely well, which strengthens this hypothesis. As will be seen below, the equation fits equally well other sets of data. The equation also fits equally well the data resulting from the two initial solutions (with and without water). Although further investigations should be

carried out (e.g. by gradually increasing the amount of water in the initial solutions), this suggests that the mechanism of particle formation is the same in both cases. We hypothesize that, the exchange rates between solvent molecules is not substantially changed, but by starting with some initial water concentration in the focused stream, reduces the amount of time needed to reach a water:ethanol ratio that induces the assembly of the lipid molecules into cubosomes, hence effectively reducing the mixing time τ . Hence, reducing the nucleation time and increasing the particles formation rate with smaller sizes. Still, this is only a speculation as more tests would be required to truly understand the dynamics in each of these processes. The hypothesis stated by eq. 9 that culminates in eq. 14 should also be refined and more scrutinized, to check for generality and bring further insight into the meaning of the constants A and B.

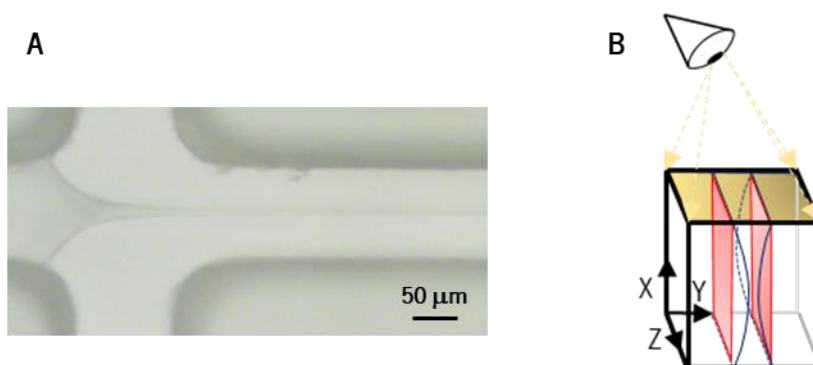


Figure 3.5: Comparison between the focused width that is seen in a microscope during the hydrodynamic focusing inside a microfluidic device, and what is the typical width profile in a cross section inside the device. A) Photograph taken in the microscope during the hydrodynamic focusing inside the COC microfluidic device. B) Schematic representation of the cross section of an hydrodynamically focused stream, highlighting the concave flow profile (blue lines). The microscope observation takes as a reference the top wall of the device, and therefore, the measured width (in red) of the focused stream corresponds to its maximum width, giving an overestimation of the average width of the focused stream.

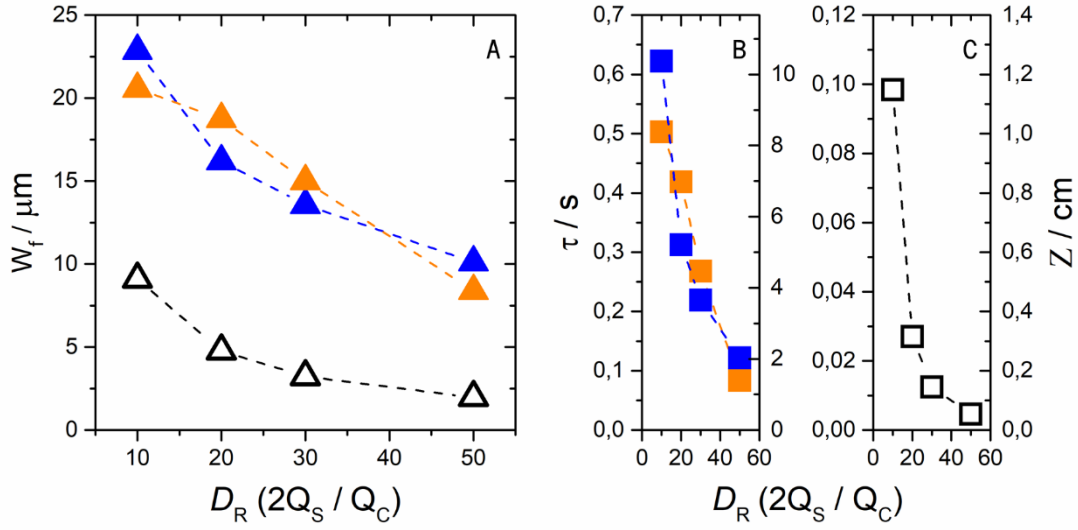


Figure 3.6: Graphical representation of the focused ethanol stripe width (w_f), and its associated mixing time (τ), and channel length needed to achieve complete mixing (Z) as a function of D_R . Here $Q_i=100 \mu\text{L}/\text{min}$ (used in the COC device). In panel A, both (\blacktriangle) and (\blacktriangle) represent the measured w_f , and (\triangle) represents the estimated w_f using Eq. 16. In panels B and C, the mixing time τ is represented in the left ordinate axis whereas mixing length Z is represented in the right ordinate axis. Both (\blacksquare) and (\blacksquare) are a representation for τ and Z obtained using the measured w_f and calculated using the Eq. 10 and 11, while (\square) represents τ and Z using the estimated w_f . The orange symbols represent the data obtained when the lipid stock solution was composed by monoolein dissolved in absolute ethanol (1/99), and the blue symbols when it was dissolved in an absolute ethanol:water mixture (1/70/29). The three graphs show a decrease of both w_f , τ and Z , when D_R (and Q_i) is increased. Note however, that the measured widths and corresponding τ and Z are significantly overestimated due to the parabolic profile of the focused stream.

3.2.2. Commercial cyclic olefin copolymer (COC) versus polydimethylsiloxane (PDMS)

In this section, we wanted to try other materials for the microfluidic device. Although COC provided interesting results, the commercial chips cost, the brittleness of the material that sometimes got broken after a few uses, and the impossibility of making new designing and produce them at our laboratory pushed the group to try out new materials.

The desired material should be easy to use and allow fast prototyping, i.e. allow fabrication of devices with novel designs, such as different channel widths and number of junctions. Furthermore, it must be chemically inert and transparent in the UV-visible region so that the flow characteristics could be monitored as the experiments proceeded. Polydimethylsiloxane (PDMS) devices possess such characteristics and so, a PDMS device with a similar design to the COC device was used.

The PDMS device used in the experiments had channels with 100 μm height and width, while the outlet microchannel length was about 3,3 cm. The sealing of the device was of glass. With a shorter channel length than the COC device, the Q_t was of 20 $\mu\text{L}/\text{min}$ to allow a larger residence time and ensure that complete mixing is achieved before the end of the channel. The Q_r of 10, 20, 30 and 50 was as before.

Before starting to flow anything inside the device, the device was washed as described in the previous section where a COC microfluidic device was used. To connect the syringes to the device, the Teflon tubes (1548L, IDEX) were directly connected to the device by plunging them inside the channel entries. The connection between syringes and the Teflon tubes was made using syringe needles (Needle, Agani™).

In this experiment we aimed at the effect that a different microfluidic device would have when forming particles and so, the solutions used to synthesize the particles were of the same composition as the ones shown in the previous section.

Because of the problems detected in section 3.1, the lipid stock solutions used could not be composed of only lipid molecules dissolved in ethanol and so, in this work only the lipid batch solutions that already contained water could be used. As for the side solution, the F127 solutions were of the same composition, i.e. the solutions prepared were the same as in Table 3.3.

The lipid stock solutions used through the course of the experiments were of monoolein dissolved in an absolute ethanol:water mixture (1/70/29). These solution batches were of the same composition as the ones used in the previous chapter in order to facilitate the comparison between the two devices.

Table 3.3 and Figure 3.7 are representations of the comparison between the sizes and associated standard deviations of the particles obtained using both microfluidic devices, PDMS and COC, at different Q_r . It is important to remind, that in this comparison using two different microfluidic devices, the Q_t used in each of them was different, since in the PDMS was of 20 $\mu\text{L}/\text{min}$ whereas on the COC was 100 $\mu\text{L}/\text{min}$.

Table 3.3: Comparison of the size parameters of particles prepared using a PDMS and a COC microfluidic device. Particles produced in the COC microfluidic device are smaller and show smaller standard deviation. The initial lipid solution has a composition of 1/70/29 lipid/ethanol/water wt%.

Q_r	F127 wt%		MO wt% final	PDMS microfluidic device			COC microfluidic device		
	initial	final		D_H / nm	Std. Dev. / nm	PDI	D_H / nm	Std. Dev. / nm	PDI
10	0.100	0.091	0.091	171	20	0.19	159	6	0.15
20	0.050	0.048	0.048	146	12	0.13	119	5	0.13
30	0.033	0.032	0.032	134	11	0.11	110	4	0.13
50	0.020	0.020	0.020	126	5	0.11	106	5	0.13

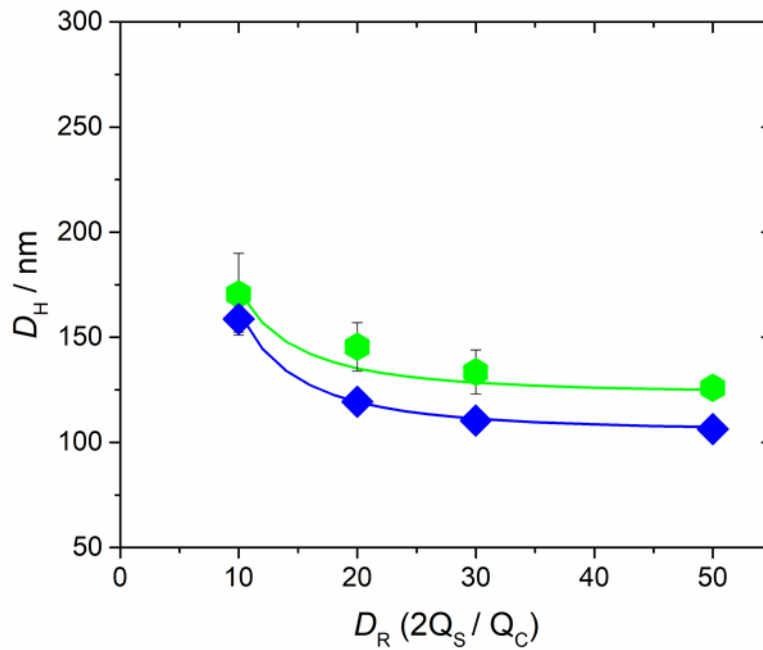


Figure 3.7: Average hydrodynamic diameter values and associated standard deviations for particles obtained using the PDMS microfluidic device (●) and the COC microfluidic device (◆) at different Q_r . The Q_r used in the PDMS microfluidic device was of 20 $\mu\text{L}/\text{min}$ whether in the COC microfluidic device was of 100 $\mu\text{L}/\text{min}$. The initial sample composition is (1/70/29) for lipid/ethanol/water wt%, and the lipid:F127 ratio is 1:1 for all Q_r . The size in both cases decreases as a function of Q_r . The sizes obtained using the COC device are smaller than the ones obtained in the PDMS device. This can be due to the different Q_r or due to the different surface properties of COC and PDMS. The solid lines represent fittings to the equation $D_H = A (D_R + 1)^{-2} + B$ (Eq. 28) with the fitting parameters A and B being 4900 and 123 for particles formed in the PDMS chip, and 5700 and 105 for particles formed using the COC microfluidic device, respectively.

The difference expressed in Figure 3.7 and Table 3.3, indicated that particles obtained using a microfluidic device made of PDMS and COC described the same behaviour, i.e. in both cases the average size of the particles was decreasing as the Q_r was increasing. Although both experiments had the same behaviour, the average size and PDI between both experiments was different. The particles produced using a PDMS microfluidic device had their average size slightly

higher than the ones obtained using the COC device. This difference was not only reflected in their average size but, it was also reflected in the standard deviation which was slightly larger in PDMS.

These differences could not be explained from a formulation point of view, since both formulations had the same composition. The two aspects that truly differed between the experiments set up was the device used and the Q_t applied in each case. The PDMS device provided the particles with the biggest average sizes. This device had a shorter channel length (3.3 cm) than the COC (8.2cm). The shorter channel length does not necessarily mean that molecules have a shorter residence time inside the microchannels, because at a Q_t of 20 $\mu\text{L}/\text{min}$ the residence time was about 0.99 sec, which was roughly twice compared to the residence time of the fluids inside the COC device (0.49sec). This difference in the residence time could partially explain the slightly different results. We propose that this extra time inside the microchannel, under the laminar flow regime conditions, could indeed have allowed the nucleation process to be extended. An additional effect could be due to the fact that at $Q_t = 20 \mu\text{L}/\text{min}$, the molecules spend more time at the cross where the three streams mix, and the width of the focused stream is narrowing down. Having the molecules spending more time in this region where the width of the focused stream is going from a large width into a narrower width could also partially explain slightly larger sizes and standard deviation. Finally, one should note also that the walls of the two devices (COC and PDMS) have somewhat different mechanical properties. In the case of COC, the walls are very rigid, whereas in the case of PDMS the walls are softer. These differences could also partially affect the flow and mixing times, resulting in slightly different particle sizes. To elucidate better each of these effects, additional studies should be performed in the future.

3.2.3. Influence of the stabilizer concentration and mixing ratio

Until this point, the focus was put on the manipulation of the flow conditions to influence the sizes of the particles formed. In this section the particle formation process is analysed from a formulation point of view.

The F127 is the most widely used stabilizer for cubosomes. The triblock copolymer composed by an average of one hundred units of polyethylene oxide (PEO) on the sides of a sixty five unit polypropylene oxide (PPO) made it suitable for coating the amphiphilic structures.²³

This polymer is usually attached to the lipidic particles by its PPO group, whose hydrophobic nature forces it to avoid interactions with polar solvents. Both of the side groups are hydrophilic,

and so they can remain at the surface of the lipid particles where they work as stabilizers, by increasing the free-energy barrier that prevents the colloidal dispersions to aggregate.²⁵

In this experiment, we intended to understand how the particles would react if the stabilizer concentration was increased. To do so, lipid stock solutions of monoolein dissolved in an absolute ethanol:water mixture were used to form particles in a PDMS device. The weight ratios of F127 to MO was 1 and 3.

In Figure 3.8, the progression of the particles size with the increase of Q_R is demonstrated. The size of particles in both cases seemed to be similar for each of the Q_R , with very slight differences observed for the two F127:MO weight ratios. As with the other experiments, the particle size decreases when D_R is increased.

At these mass ratios the F127 molecules were not influencing the dispersions size because, at these ratios the cubosomes were already coated. To understand better this idea, a simple calculation for an approximate number of molecules needed of F127 to coat the cubosomes was performed. In this calculation, approximations of the true values were considered, since once in solution it was not possible to predict the exact values.

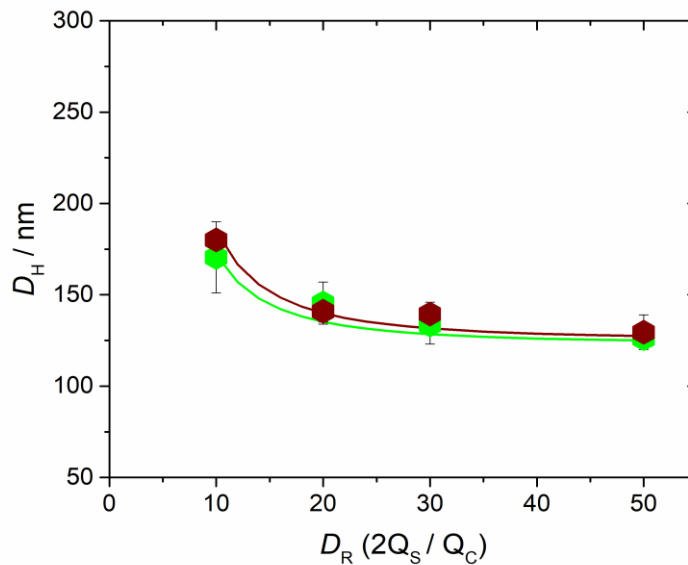


Figure 3.8: Influence of the lipid:F127 mixing ratio on the average hydrodynamic diameters. The (●) represent the average sizes of the particles produced with F127 side solutions at a constant mass ratio of 1 and the (●) represent the ones produced with F127 side solutions at a constant mass ratio of 3. The size of the two types of particles created decreases as the Q_R increases without noticeable differences for the two lipid:F127 mass ratios. The solid lines represent fittings to the equation $D_H = A(D_R + 1)^2 + B$ (Eq. 28) with the fitting parameters A and B being 6000 and 125 for particles formed using a F127:MO mass ratio of 3, and 4900 and 123 for particles formed at a F127:MO mass ratio of 1, respectively.

The area considered for each cubosome was calculated for a cubosome edge length of 150 nm and so, the area determined for the surface of the cubosome was ca. $6 \times (150 \times 10^{-9})^2 = 1.35 \times 10^{-13} \text{ m}^2$. With the value for the area of each cubosome, the determination of the total area that the F127 molecules had to coat was estimated. To calculate the total area, one needs to estimate the approximate number of cubosomes in solution. For this we consider that the composition of the cubic phase has (as an approximation, which is corroborated by the phase diagram) ca. 42 wt% water and 58 wt% monoolein. Hence, our most concentrated cubosome solution, by having 0.1 wt% monoolein, has ca. 0.17 wt% cubosomes. Assuming for simplicity equal densities of lipid and water, dividing the resultant volume fraction of 0.17 vf% by the volume of a cubosome ($(150 \times 10^{-9})^3 \text{ m}^3$) results in ca. 5×10^{17} cubosomes per cubic meter. This results in a total cubosome facet area of $6.8 \times 10^4 \text{ m}^2$ per cubic meter of solution.

Assuming as an approximation that the PPO section of one F127 molecule occupies an area of 20 nm^2 of the cubosome surface, results in ca. 3.4×10^{12} spots on the cubosome surface that F127 molecules can coat. For a MW of F127 of 12.6 kDa, the number of F127 molecules in a cubic meter for 0.1 wt% F127 is ca. 4.8×10^{19} , which is several orders of magnitude greater than spots available in the cubosome facets to coat. These values showed that, in both cases the number of F127 molecules were largely above what was required to coat the cubosome particles, which partially justifies the small differences between the two F127:MO ratios.

3.2.4. Increase in the lipid concentration

The increase in lipid concentration was also considered when formulating the lipid stock solutions. In this chapter the lipid concentration in the lipid stock solution was increased to 3 wt% and 5 wt%. This increase in the lipid concentration is desirable to provide more versatility and to provide more concentrated samples. It also provides a hint into how scalable this approach can be and how concentration changes could impact the average size of the final particles.

In this experiment, the COC microfluidic device was used. Both lipid stock solutions, 3 wt% and 5 wt%, had their F127 side solutions with the concentration adjusted. These changes in the solution concentrations are depicted below in *Table 3.4* and *Table 3.5*.

Table 3.4: Solvent shifting results for an initial monoolein concentration of 3 wt%. The final lipid:F127 mass ratio is 2 and kept constant for the different Q_k . The used microfluidic device is the COC. The particles obtained were from different lipid batches, one of monoolein 3 wt% dissolved in absolute ethanol and the other of monoolein dissolved in an absolute ethanol:water mixture (3/70/27). At these higher initial lipid concentrations the size standard deviation and PDI increases. Again, similarly to the more dilute lipid cases, the average size, size standard deviation, and PDI were smaller for particles where the lipid stock solution contained water.

Q_k	F127 wt%		MO wt% final	MO/C ₂ H ₆ O			MO/C ₂ H ₆ O/H ₂ O		
	initial	final		D_H / nm	Std. Dev. / nm	PDI	D_H / nm	Std. Dev. / nm	PDI
10	0.60	0.55	0.27	299	111	0.60	162	15	0.29
20	0.30	0.29	0.14	230	85	0.50	158	16	0.23
30	0.20	0.19	0.10	204	54	0.24	152	17	0.19
50	0.12	0.12	0.06	183	1	0.20	148	11	0.18

Table 3.5: Solvent shifting results for an initial monoolein concentration of 5 wt%. The final lipid:F127 mass ratio is 2 and kept constant for the different Q_k . The used microfluidic device is the COC. The particles obtained were from different lipid batches, one of monoolein 5 wt% dissolved in absolute ethanol and the other of monoolein dissolved in an absolute ethanol:water mixture (5/70/25). At such high initial lipid concentrations the production of the cubosome particles seems to become uncontrolled, leading to erratic trends in the sizes.

Q_k	F127 wt%		MO wt% final	MO/C ₂ H ₆ O			MO/C ₂ H ₆ O/H ₂ O		
	initial	final		D_H / nm	Std. Dev. / nm	PDI	D_H / nm	Std. Dev. / nm	PDI
10	1.00	0.91	0.45	86	-	-	168	51	0.50
20	0.50	0.48	0.24	59	-	-	323	174	0.38
30	0.33	0.32	0.16	150	-	-	474	39	1.1
50	0.20	0.20	0.10	102	-	-	57	-	-

The increase in the lipid concentration when forming particles in microfluidic devices is usually associated with an increase in the particles production. However, Figure 3.9 shows that an increase in the concentration was translated into a loss of control over the particles size. This was more noticeable for initial lipid concentrations of 5 wt%, where the usual trend in particle size (particle size decreasing as the Q_k is increased) was entirely lost, along with the observation of much larger standard deviation values, which showed that the reproducibility of the experiments was compromised. For the intermediate case of initial lipid concentrations of 3 wt% some control was still achieved as visible in Figure 3.9.

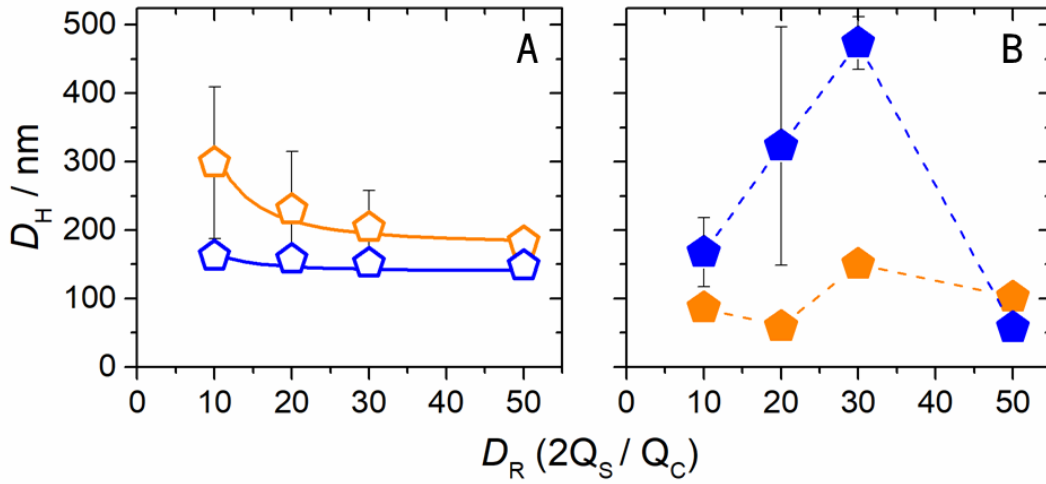


Figure 3.9: Influence of the lipid concentration on the average size of particles obtained using a COC microfluidic device at a Q of 100 $\mu\text{l}/\text{min}$. A) Average sizes of particles obtained from a lipid stock solution with Monoolein at 3 wt%. B) Average sizes of particles obtained from a lipid stock solution with Monoolein at 5 wt%. The orange symbols represent the data obtained when the lipid stock solution was composed by monoolein dissolved in absolute ethanol (1/99), and the blue symbols when it was dissolved in an absolute ethanol:water mixture (1/70/29). The solid lines represent fittings to the equation $D_H = A(D_R + 1)^{-2} + B$ (Eq. 28) with the fitting parameters A and B of 13500 and 180 for monoolein:ethanol, and 2700 and 180 for the monoolein:ethanol:water initial solutions, respectively. The dashed lines are guides to the eye. The increase in lipid concentration leads to a poorer size control with microfluidics. At 3 wt% lipid some control over the size is still achieved.

The loss of the control over the particles formation was also demonstrated when forming liposomes using high concentration lipid solutions. In the work presented by Albino et al., they suggested that the formation of liposomes with uncontrolled sizes was explained by the short time required for mixing ethanol and water, this short time wasn't enough to allow all the lipid molecules to assemble which resulted in the formation of some uncontrolled sized liposomes.⁷³

The lipid concentration that was being applied in our experience seemed to form the same kind of results. In fact, with the decrease in the lipid concentration down to 3 wt%, it was possible to achieve some control over the particle sizes, especially in the case where no water was used.

We proposed that a similar case compared to the one described in above was occurring during our experiments. In the first section of the results we proposed that the use of water in the lipid batch solutions was responsible for decreasing the time required for the lipid to assemble into particles, increasing the nucleation rate and decreasing particle size. In this case, with the lipid concentration significantly higher, decreasing this mixing time led to a more uncontrolled process, with the particles resulting from initial lipid solutions containing water showing more scattered sizes throughout the D_R range (Figure 3.9).

3.2.5. DODAB:MO in liposome formation

The conjugation of more than one lipid to form lipid nanoparticles is widely used. In this experiment, it was intended to use two different lipid molecules to form liposomes. The cationic Dioctadecyldimethylammonium bromide, commonly referred as DODAB, and the neutral lipid monoolein (MO), have both been associated to produce liposomes used for gene therapy.^{42,74}

The positively charged DODAB promotes the compaction of nucleic acids, whereas the MO works as a fluidizing agent that enables the escape of the liposomes content from the endosomes and lowers the toxicity of the cationic carriers.⁷⁴

In this section, it was intended to form liposome particles using the COC microfluidic device. To produce these particles, two lipid molar ratio between monoolein and DODAB were chosen. The chosen ratios were of DODAB:MO at 2:1 and DODAB:MO at 1:2.

The lipid stock solutions consisted on the mixture of DODAB:MO at two different ratios, 2:1 and 1:2, in both solutions the lipid mixture was at 1 wt% dissolved in absolute ethanol. As for the flow conditions, the Q_c used was 100 $\mu\text{l}/\text{min}$ and the Q_d used were of 10, 20, 30 and 50.

After trying to form liposomes using the lipid batch solution of DODAB:MO at 2:1, it was noted that the microchannels of the device had precipitated structures in the channel walls, Figure 3.10. The occurrence of this type of precipitated structures was likely the result of the poor solubility of DODAB when it contacted with the water side solutions. The occurrence of structures in the side channels is also an indicator of DODAB's poor solubility. Once the flow stopped, the centre stream had partially entered in the side channels where the F127 side solutions resided and that promoted the precipitation of DODAB.

The lipid batch solution of DODAB:MO at 1:2 did not show the same behaviour when it was injected in the microchannels of the COC device. This could be explained by the relation between MO and DODAB, since in this case monoolein was at a higher molar ratio, it could be fluidizing the system. This type of behaviour between DODAB:MO was described in another work, where it was demonstrated that MO had a similar effect to on DODAB as the increase in the temperature.⁴²

However, the average sizes obtained for the particles were somewhat inconclusive. The DLS showed autocorrelation function profiles with significant polydispersity that did not allow a proper fitting of the results.

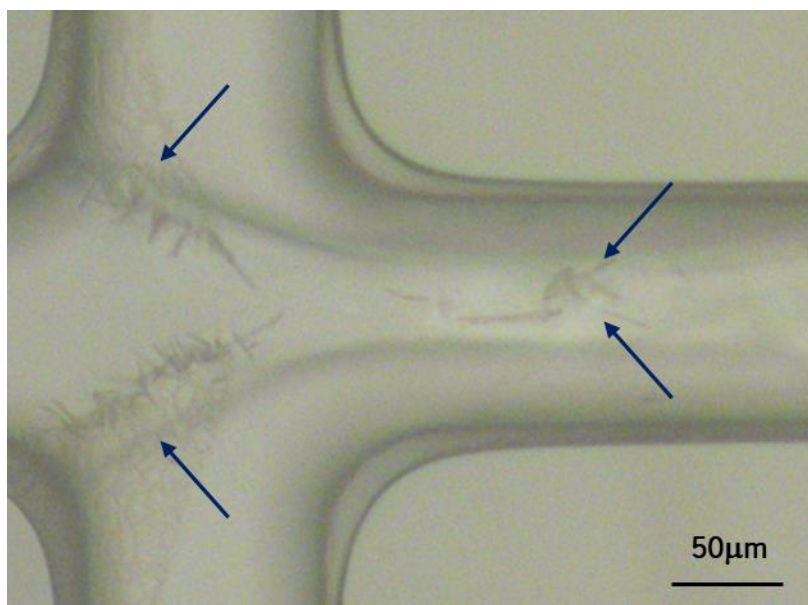


Figure 3.10: Microscope image of the COC device with strange structures precipitated inside the microchannels, when the flow of the centre lipid solution, of DODAB:MO (2:1) and side solutions of F127, was stopped. The presence of structures inside the microchannels are indicated by the blue arrows.

In Table 3.6, the average sizes showed no control over the particles formation. Unlike what was demonstrated until now in the first sections of the present work. The particles obtained here did not follow the assumptions shown previously, i.e. the monodispersity in sample sizes and the decrease in size as Q_k was increased. Figure 3.10.

Table 3.6: Average sizes with associated standard deviation, and PDI for the particles formed in a COC microfluidic device at different Q_k . Both D_H and PDI were indicating that the results were a consequence of the loss of control over the particles that were being formed.

Q_k	DODAB:MO:C ₂ H ₆ O		
	D_H / nm	Std. Dev. / nm	PDI
10	5055	1777	2.12
20	5576	1649	1.82
30	1014	1010	1.96
50	4505	1585	1.92

These enormous sizes obtained when using lipid concentrations around 1 wt% were seen in previous work, where low concentrations of the same lipid mixtures were used and demonstrated that, when using concentrations close to the ones we used, the liposomes tend to acquire significant increases in size. This increase in size could be related to a structural change in the liposome structures or to the coexistence of two different populations of particles.⁷⁵

Chapter 4 - Conclusion and future perspectives

The drug delivery approaches on new therapies is promising. However, the protocols to produce these systems provide reduced control over the particles formation, which generally results on polydisperse particles. Thus, in this work we intended to develop a method that allowed us to tune these particles while keeping them relatively monodisperse.

The microfluidic systems were the strategy chosen but to use it some considerations needed to be considered. One of the aspects we were able to demonstrate was the influence of the materials used, as the use of a PDMS microfluidic device proved to not be ideal for the solvents chosen. Since whether mixing either absolute ethanol, or IPA, and water, unexpected structures started to form, which led to their precipitation on the microchannel walls. Such kind of impurities can have a strong impact in the analysis techniques or even at cell viability assays when testing particles produced in these devices.

As for the particles, we managed to produce cubosome particles combining a solvent shifting technique with microfluidic hydrodynamic focusing. Compared with bulk, microfluidics allowed to tune the particle size by manipulating the flow rate ratio. Different lipid concentrations and compositions, different stabilizer concentrations, different microfluidic devices, and the mixture of DODAB:MO at two different molar ratios, 2:1 and 1:2, were also tested.

We were able to demonstrate that, when using a microfluidic device control over the particles size was obtained if using a lipid concentration of 1 wt%. Moreover, it was also demonstrated that by changing the Q_R it is possible to tune the particles size, obtaining smaller particles as the Q_R is increased. However, using a superior lipid concentration led to uncontrolled sized cubosomes. The opposite was observed if using different stabilizer concentrations, where the size of the cubosome particles did not demonstrate significant changes. The inclusion of water in the lipid stock solutions resulted in smaller cubosome particles. The DODAB:MO mixture, at a molar ratio of 2:1 led to the precipitation of DODAB inside the microchannels and at a molar ratio of 1:2 led to large and uncontrolled size particles.

The microfluidic approach on the particle formation seems to be promising, as the control over particle formation was demonstrated. Still, new studies to understand what is the exact internal structure of particles are required, for this Small Angle X-Ray (SAXS) and Cryo-Transmission Electronic Microscopy (Cryo-TEM) should be used. The design of a 3-D microfluidic device should be also tested, which would allow a 3-D focusing possibly reducing even more the size dispersity

of the particles and maybe allowing the use of more concentrated lipid solutions. Certainly, the use of microfluidics to tailor the size and structure of drug-delivery systems opens a plethora of new possibilities.

As for the particles, encapsulation studies of relevant molecules and tests on cell lines should be made to study their efficiency. Especially now that we have some control over the particles size, we could study how the size influences cellular trafficking and therapeutic efficiency.

Chapter 5 – Bibliography

- (1) Akbarzadeh, A.; Rezaei-sadabady, R.; Davaran, S.; Joo, S. W.; Zarghami, N.; Hanifepour, Y.; Samiei, M.; Kouhi, M.; Nejati-Koshki, K. Liposome: Classification, Preparation, and Applications. *Nanoscale Res. Lett.* **2013**, *8*, 102.
- (2) Zhang, L.; Gu, F.; Chan, J.; Wang, A. Z.; Langer, R. S.; Farokhzad, O. C. Nanoparticles in Medicine: Therapeutic Applications and Developments. *Transl. Med.* **2008**, *83* (5), 761–769.
- (3) Rawat, M.; Singh, D.; Saraf, S.; Saraf, S. Nanocarriers: Promising Vehicle for Bioactive Drugs. *Biol. Pharm. Bull.* **2006**, *29* (9), 1790–1798.
- (4) Tadros, T. *Encyclopedia of Colloid and Interface Science*; 2013.
- (5) Silva, B. F. B. Phase Behavior of Asymmetric Catanionic Surfactants: Equilibrium, Phase Transitions and Microstructure. **2009**, 1–362.
- (6) Coppola, L.; Gianferri, R.; Nicotera, I.; Oliviero, C.; Ranieri, G. A. Structural Changes in CTAB/H₂O Mixtures Using a Rheological Approach. *PCCP* **2004**, *6*, 2364–2372.
- (7) Holmberg, K.; Bo, J.; Kronberg, B. *Surfactants and Polymers in Aqueous Solution, 2nd Edition*, John Wiley and Sons Ltd. West Sussex, UK; 2003.
- (8) Hamley, I. W. *Introduction to Soft Matter– Revised Edition*; 2007.
- (9) Larsson, K. Cubic Lipid-Water Phases: Structures and Biomembrane Aspects. *J. Phys. Chem.* **1989**, *93* (21), 7304–7314.
- (10) Lancelot, A.; Sierra, T.; Serrano, J. L. Nanostructured Liquid-Crystalline Particles for Drug Delivery. *Expert Opin. Drug Deliv.* **2014**, *11* (4), 547–564.
- (11) Gustafsson, J.; Ljusberg-Wahren, H.; Almgren, M.; Larsson, K. Cubic Lipid–Water Phase Dispersed into Submicron Particles. *Langmuir* **1996**, *12* (20), 4611–4613.
- (12) Zhao, X. Y.; Zhang, J.; Zheng, L. Q.; Li, D. H. Studies of Cubosomes as a Sustained Drug Delivery System. *J. Dispers. Sci. Technol.* **2004**, *25* (6), 795–799.
- (13) Seddon, J. M.; Templer, R. H. Polymorphism of Lipid-Water Systems. In *Handbook of Biological Physics*; 1995; Vol. 1, pp 97–160.
- (14) Fong, C.; Le, T.; Drummond, C. J. Lyotropic Liquid Crystal Engineering-Ordered Nanostructured Small Molecule Amphiphile Self-Assembly Materials by Design. *Chem. Soc. Rev.* **2012**, *41* (3), 1297–1322.
- (15) Kulkarni, C. V.; Wachter, W.; Iglesias-Salto, G.; Engelskirchen, S.; Ahualli, S. Monoolein: A

- Magic Lipid? *Phys. Chem. Chem. Phys.* **2011**, *13* (8), 3004–3021.
- (16) Ganem-Quintanar, A.; Quintanar-Guerrero, D.; Buri, P. Monoolein: A Review of the Pharmaceutical Applications. *Drug Dev. Ind. Pharm.* **2000**, *26* (8), 809–820.
 - (17) Qiu, H.; Caffrey, M. The Phase Diagram of the Monoolein/Water System: Metastability and Equilibrium Aspects. *Biomaterials* **2000**, *21* (3), 223–234.
 - (18) Silva, J.; Oliveira, A. C. N.; Gomes, A.; Oliveira, M. Development of Dioctadecyldimethylammonium Bromide/Monoolein Liposomes for Gene Delivery. *Cell Interact.* **2012**, 245–272.
 - (19) Silva, J. P. N.; Oliveira, A. C. N.; Casal, M. P. P. A.; Gomes, A. C.; Coutinho, P. J. G.; Coutinho, O. P.; Oliveira, M. E. C. D. R. DODAB:Monoolein-Based Lipoplexes as Non-Viral Vectors for Transfection of Mammalian Cells. *Biochim. Biophys. Acta - Biomembr.* **2011**, *1808* (10), 2440–2449.
 - (20) Huang, Y.; Gui, S. Factors Affecting the Structure of Lyotropic Liquid Crystals and the Correlation between Structure and Drug Diffusion. *RSC Adv.* **2018**, *8* (13), 6978–6987.
 - (21) Serieye, S.; Méducin, F.; Milošević, I.; Fu, L.; Guillot, S. Interface Tuning and Stabilization of Monoglyceride Mesophase Dispersions: Food Emulsifiers and Mixtures Efficiency. *J. Colloid Interface Sci.* **2017**, *496*, 26–34.
 - (22) Honda, T.; Miyazaki, M.; Nakamura, H.; Maeda, H. Controllable Polymerization of N-Carboxy Anhydrides in a Microreaction System. *Lab Chip* **2005**, *5* (8), 812–818.
 - (23) Chong, J. Y. T.; Mulet, X.; Postma, A.; Keddie, D. J.; Waddington, L. J.; Boyd, B. J.; Drummond, C. J. Novel RAFT Amphiphilic Brush Copolymer Steric Stabilisers for Cubosomes: Poly(Octadecyl Acrylate)-Block-Poly(Polyethylene Glycol Methyl Ether Acrylate). *Soft Matter* **2014**, *10* (35), 6666–6676.
 - (24) Mo, J.; Milleret, G.; Nagaraj, M. Liquid Crystal Nanoparticles for Commercial Drug Delivery. *Liq. Cryst. Rev.* **2017**, *5* (2), 69–85.
 - (25) Nakano, M.; Sugita, A.; Matsuoka, H.; Handa, T. Small-Angle X-Ray Scattering and ¹³C NMR Investigation on the Internal Structure of “Cubosomes.” *Langmuir* **2001**, *17* (13), 3917–3922.
 - (26) Siekmann, B.; Bunjes, H.; Koch, M. H. J.; Westesen, K. Preparation and Structural Investigations of Colloidal Dispersions Prepared from Cubic Monoglyceride-Water Phases. *Int. J. Pharm.* **2002**, *244* (1–2), 33–43.
 - (27) Bose, S.; Michniak-Kohn, B. Preparation and Characterization of Lipid Based Nanosystems

- for Topical Delivery of Quercetin. *Eur. J. Pharm. Sci.* **2013**, *48* (3), 442–452.
- (28) Berger, N.; Sachse, A.; Bender, J. Filter Extrusion of Liposomes Using Different Devices: \rcomparison of Liposome Size, Encapsulation Efficiency, And\rprocess Characteristics. *Int. J. Pharm.* **2001**, *223*, 55–68.
 - (29) Garg, G.; Saraf, S.; Saraf, S. Cubosomes: An Overview. *Biol. Pharm. Bull.* **2007**, *30* (2), 350–353.
 - (30) Karami, Z.; Hamidi, M. Cubosomes: Remarkable Drug Delivery Potential. *Drug Discov. Today* **2016**, *21* (5), 789–801.
 - (31) Spicer, P. T.; Hayden, K. L.; Lynch, M. L.; Ofori-Boateng, A.; Burns, J. L. Novel Process for Producing Cubic Liquid Crystalline Nanoparticles (Cubosomes). *Langmuir* **2001**, *17* (19), 5748–5756.
 - (32) Nakano, M.; Teshigawara, T.; Sugita, A.; Leesajakul, W.; Taniguchi, A.; Kamo, T.; Matsuoka, H.; Handa, T. Dispersions of Liquid Crystalline Phases of the Monoolein/Oleic Acid/Pluronic F127 System. *Langmuir* **2002**, *18* (24), 9283–9288.
 - (33) Chong, J. Y. T.; Mulet, X.; Waddington, L. J.; Boyd, B. J.; Drummond, C. J. Steric Stabilisation of Self-Assembled Cubic Lyotropic Liquid Crystalline Nanoparticles: High Throughput Evaluation of Triblock Polyethylene Oxide-Polypropylene Oxide-Polyethylene Oxide Copolymers. *Soft Matter* **2011**, *7* (10), 4768–4777.
 - (34) Guillot, S.; Salentinig, S.; Chemelli, A.; Sagalowicz, L.; Leser, M. E.; Glatter, O. Influence of the Stabilizer Concentration on the Internal Liquid Crystalline Order and the Size of Oil-Loaded Monolinolein-Based Dispersions. *Langmuir* **2010**, *26* (9), 6222–6229.
 - (35) Oka, T.; Hasan, M.; Islam, M. Z.; Moniruzzaman, M.; Yamazaki, M. Low-PH-Induced Lamellar to Bicontinuous Primitive Cubic Phase Transition in Dioleoylphosphatidylserine/Monoolein Membranes. *Langmuir* **2017**, *33* (43), 12487–12496.
 - (36) Tran, N.; Mulet, X.; Hawley, A. M.; Fong, C.; Zhai, J.; Le, T. C.; Ratcliffe, J.; Drummond, C. J. Manipulating the Ordered Nanostructure of Self-Assembled Monoolein and Phytantriol Nanoparticles with Unsaturated Fatty Acids. *Langmuir* **2018**, *34* (8), 2764–2773.
 - (37) Whitesides, G. M. The Origins and the Future of Microfluidics. *Nature* **2006**, *442* (7101), 368–373.
 - (38) Squires M., T.; Quake R., S. Microfluidics: Fluid Physics at the Nanoliter Scale. *Rev. Mod. Phys.* **2005**, *77* (3), 977–1026.

- (39) Stone, H. A.; Stroock, A. D.; Ajdari, A. Engineering Flows in Small Devices. *Annu. Rev. Fluid Mech.* **2004**, *36* (1), 381–411.
- (40) Jahn, A.; Vreeland, W. N.; Gaitan, M.; Locascio, L. E. Controlled Vesicle Self-Assembly in Microfluidic Channels with Hydrodynamic Focusing. *J. Am. Chem. Soc.* **2004**, *126* (9), 2674–2675.
- (41) Van Swaay, D.; Demello, A. Microfluidic Methods for Forming Liposomes. *Lab Chip* **2013**, *13* (5), 752–767.
- (42) Oliveira, I. M. S. C.; Silva, J. P. N.; Feitosa, E.; Marques, E. F.; Castanheira, E. M. S.; Real Oliveira, M. E. C. D. Aggregation Behavior of Aqueous Dioctadecyldimethylammonium Bromide/Monoolein Mixtures: A Multitechnique Investigation on the Influence of Composition and Temperature. *J. Colloid Interface Sci.* **2012**, *374* (1), 206–217.
- (43) Lu, M.; Ozcelik, A.; Grigsby, C. L.; Zhao, Y.; Guo, F.; Leong, K. W.; Huang, T. J. Microfluidic Hydrodynamic Focusing for Synthesis of Nanomaterials. *Nano Today* **2016**, *11* (6), 778–792.
- (44) Yang, Z.; Matsumoto, S.; Goto, H.; Matsumoto, M.; Maeda, R. Ultrasonic Micromixer for Microfluidic Systems. *Sensors Actuators, A Phys.* **2001**, *93* (3), 266–272.
- (45) Meijer, H. E. H.; Singh, M. K.; Kang, T. G.; Den Toonder, J. M. J.; Anderson, P. D. Passive and Active Mixing in Microfluidic Devices. *Macromol. Symp.* **2009**, *279* (1), 201–209.
- (46) Mansur, E. A.; YE, M.; WANG, Y.; DAI, Y. A State-of-the-Art Review of Mixing in Microfluidic Mixers. *Chinese J. Chem. Eng.* **2008**, *16* (4), 503–516.
- (47) Luong, T.-D.; Phan, V.-N.; Nguyen, N.-T. High-Throughput Micromixers Based on Acoustic Streaming Induced by Surface Acoustic Wave. *Microfluid Nanofluid* **2011**, *10*, 619–625.
- (48) Stroock, A. D.; Dertinger, S. K. W.; Ajdari, A.; Mezić, I.; Stone, H. A.; Whitesides, G. M. Chaotic Mixer for Microchannels. *Science (80-)*. **2002**, *295* (5555), 647–651.
- (49) Knight, J. B.; Vishwanath, A.; Brody, J. P.; Austin, R. H. Hydrodynamic Focusing on a Silicon Chip: Mixing Nanoliters in Microseconds. *Phys. Rev. Lett.* **1998**, *80* (17), 3863–3866.
- (50) Simonnet, C.; Groisman, A. Two-Dimensional Hydrodynamic Focusing in a Simple Microfluidic Device. *Appl. Phys. Lett.* **2005**, *87* (11), 85–88.
- (51) Lee, G. B.; Chang, C. C.; Huang, S. B.; Yang, R. J. The Hydrodynamic Focusing Effect inside Rectangular Microchannels. *J. Micromechanics Microengineering* **2006**, *16* (5), 1024–1032.
- (52) Microchannels, P. P.; Sundararajan, N.; Pio, M. S.; Lee, L. P.; Berlin, A. A. Three-

- Dimensional Hydrodynamic Focusing In. **2004**, *13* (4), 559–567.
- (53) Park, J. Il; Saffari, A.; Kumar, S.; Günther, A.; Kumacheva, E. Microfluidic Synthesis of Polymer and Inorganic Particulate Materials. *Annu. Rev. Mater. Res.* **2010**, *40* (1), 415–443.
 - (54) Anna, S. L.; Bontoux, N.; Stone, H. A. Formation of Dispersions Using “Flow Focusing” in Microchannels. *Appl. Phys. Lett.* **2003**, *82* (3), 364–366.
 - (55) Ward, T.; Faivre, M.; Abkarian, M.; Stone, H. A. Microfluidic Flow Focusing: Drop Size and Scaling in Pressure versus Flow-Rate-Driven Pumping. *Electrophoresis* **2005**, *26* (19), 3716–3724.
 - (56) Christopher, G. F.; Anna, S. L. Microfluidic Methods for Generating Continuous Droplet Streams. *J. Phys. D. Appl. Phys.* **2007**, *40* (19).
 - (57) Thorsen, T.; Roberts, R. W.; Arnold, F. H.; Quake, S. R. Dynamic Pattern Formation in a Vesicle-Generating Microfluidic Device. *Phys. Rev. Lett.* **2001**, *86* (18), 4163–4166.
 - (58) Balbino, T. A.; Azzoni, A. R.; De la Torre, L. G. Microfluidic Devices for Continuous Production of PDNA/Cationic Liposome Complexes for Gene Delivery and Vaccine Therapy. *Colloids Surfaces B Biointerfaces* **2013**, *111*, 203–210.
 - (59) Dashtimoghadam, E.; Mirzadeh, H.; Taromi, F. A.; Nyström, B. Microfluidic Self-Assembly of Polymeric Nanoparticles with Tunable Compactness for Controlled Drug Delivery. *Polymer (Guildf)*. **2013**, *54* (18), 4972–4979.
 - (60) Baby, T.; Liu, Y.; Middelberg, A. P. J.; Zhao, C. X. Fundamental Studies on Throughput Capacities of Hydrodynamic Flow-Focusing Microfluidics for Producing Monodisperse Polymer Nanoparticles. *Chem. Eng. Sci.* **2017**, *169*, 128–139.
 - (61) Rhee, M.; Valencia, P. M.; Rodriguez, M. I.; Langer, R.; Farokhzad, O. C.; Karnik, R. Synthesis of Size-Tunable Polymeric Nanoparticles Enabled by 3D Hydrodynamic Flow Focusing in Single-Layer Microchannels. *Adv. Mater.* **2011**, *23* (12), 79–83.
 - (62) Koh, C. G.; Zhang, X.; Liu, S.; Golan, S.; Yu, B.; Yang, X.; Guan, J.; Jin, Y.; Talmon, Y.; Muthusamy, N.; et al. Delivery of Antisense Oligodeoxyribonucleotide Lipopolyplex Nanoparticles Assembled by Microfluidic Hydrodynamic Focusing. *J. Control. Release* **2010**, *141* (1), 62–69.
 - (63) Valencia, P. M.; Basto, P. A.; Zhang, L.; Rhee, M.; Langer, R.; Farokhzad, O. C.; Karnik, R. Single-Step Assembly of Homogenous Lipid-Polymeric and Lipid-Quantum Dot Nanoparticles Enabled by Microfluidic Rapid Mixing. *ACS Nano* **2010**, *4* (3), 1671–1679.

- (64) Jahn, A.; Stavis, S. M.; Hong, J. S.; Vreeland, W. N.; Devoe, D. L.; Gaitan, M. Microfluidic Mixing and the Formation of Nanoscale Lipid Vesicles. *ACS Nano* **2010**, *4* (4), 2077–2087.
- (65) Duffy, D. C.; McDonald, J. C.; Schueller, O. J. A.; Whitesides, G. M. Rapid Prototyping of Microfluidic Systems in Poly(Dimethylsiloxane). *Anal. Chem.* **1998**, *70* (23), 4974–4984.
- (66) Wu, Z.; Hjort, K. Surface Modification of PDMS by Gradient-Induced Migration of Embedded Pluronic. *Lab Chip* **2009**, *9* (11), 1500–1503.
- (67) Zhou, J.; Khodakov, D. A.; Ellis, A. V.; Voelcker, N. H. Surface Modification for PDMS-Based Microfluidic Devices. *Electrophoresis* **2012**, *33* (1), 89–104.
- (68) Amiji, M.; Park, K. Prevention of Protein Adsorption and Platelet Adhesion on Surfaces by PEO/PPO/PEO Triblock Copolymers. *Biomaterials* **1992**, *13* (10), 682–692.
- (69) Ismagilov, R. F.; Stroock, A. D.; Kenis, P. J. A.; Whitesides, G.; Stone, H. A. Experimental and Theoretical Scaling Laws for Transverse Diffusive Broadening in Two-Phase Laminar Flows in Microchannels. *Appl. Phys. Lett.* **2000**, *76* (17), 2376–2378.
- (70) Mailer, A. G.; Clegg, P. S.; Pusey, P. N. Particle Sizing by Dynamic Light Scattering: Non-Linear Cumulant Analysis. *Journal Phys. Condens. Matter* **2015**, *27*, 1–8.
- (71) Puthusserickal, H.; Suman, R.; Gunjan, V. Making Sense of Brownian Motion: Colloid Characterization by Dynamic Light Scattering. *Langmuir* **2015**, *31* (1), 3–12.
- (72) Frisken, B. J. Revisiting the Method of Cumulants for the Analysis of Dynamic Light-Scattering Data. *Appl. Opt.* **2001**, *40* (24), 4087.
- (73) Balbino, T. A.; Aoki, N. T.; Gasperini, A. A. M.; Oliveira, C. L. P.; Azzoni, A. R.; Cavalcanti, L. P.; de la Torre, L. G. Continuous Flow Production of Cationic Liposomes at High Lipid Concentration in Microfluidic Devices for Gene Delivery Applications. *Chem. Eng. J.* **2013**, *226*, 423–433.
- (74) Oliveira, A. C. N.; Nogueira, S. S.; Gonçalves, O.; Cerqueira, M. F.; Alpuim, P.; Tovar, J.; Rodriguez-Abreu, C.; Brezesinski, G.; Gomes, A. C.; Lúcio, M.; et al. Role of Counter-Ion and: Helper Lipid Content in the Design and Properties of Nanocarrier Systems: A Biophysical Study in 2D and 3D Lipid Assemblies. *RSC Adv.* **2016**, *6* (53), 47730–47740.
- (75) Silva, J. P. N.; Oliveira, M. E. C. D. R.; Coutinho, P. J. G. Characterization of Mixed DODAB/Monoolein Aggregates Using Nile Red as a Solvatochromic and Anisotropy Fluorescent Probe. *J. Photochem. Photobiol. A Chem.* **2009**, *203* (1), 32–39.